EFFECT OF TEMPERATURE DEPENDENT VISCOSITY ON ENTROPY GENERATION IN TRANSIENT VISCOELASTIC POLYMERIC FLUID FLOW FROM AN ISOTHERMAL VERTICAL PLATE

G. Janardhana Reddy[1, *], Mahesh Kumar[1] and **O. Anwar Beg[2]**

[1]*Department of Mathematics, Central University of Karnataka, Kalaburagi, India.*
[2]*Fluid Mechanics, Aeronautical and Mechanical Engineering Department, School of Computing, Science and Engineering, University of Salford, Manchester M54WT, UK*

[*]*Corresponding author- Email:* gjr@cuk.ac.in *Tel number:* +91 9491472461, Kalaburagi, India

ABSTRACT: A numerical investigation of the viscosity variation effect upon entropy generation in time-dependent viscoelastic polymeric fluid flow and natural convection from a semi-infinite vertical plate is described. The Reiner-Rivlin second order differential model is utilized which can predict normal stress differences in dilute polymers. The conservation equations for heat, momentum and mass are normalized with appropriate transformations and the resulting unsteady nonlinear coupled partial differential equations are elucidated with the well-organized unconditionally stable implicit Crank-Nicolson finite difference method subject to suitable initial and boundary conditions. Average values of wall shear stress and Nusselt number, second-grade fluid flow variables conferred for distinct values of physical parameters. Numerical solutions are presented to examine the entropy generation and Bejan number along with their contours. The outcomes show that entropy generation parameter and Bejan number both increase with increasing values of group parameter and Grashof number. The present study finds applications in geothermal engineering, petroleum recovery, oil extraction and thermal insulation, etc.

KEYWORDS: *Second-grade fluid; entropy generation; free convection; Bejan number; vertical flat plate; implicit method; thermal polymer processing.*

NOMENCLATURE

Be   Bejan number

Br	Brinkman number
c_p	specific heat at constant pressure ($J\,kg^{-1}\,K^{-1}$)
$\overline{C_f}$	average dimensionless wall shear stress
k	thermal conductivity ($Wm^{-1}\,K^{-1}$)
g	acceleration due to gravity (ms^{-2})
Ns	dimensionless entropy heat generation number
$\overline{Nu}$	average Nusselt number
Pr	Prandtl number
Gr	Grashof number
t'	time (s)
t	dimensionless time
T'	temperature (K)
T	dimensionless temperature
u, v	velocity components in (x, y) coordinate system (ms^{-1})
U, V	dimensionless velocity components in X, Y directions, respectively
X	dimensionless axial coordinate
x	axial coordinate
y	transverse coordinate
Y	dimensionless transverse coordinate

Greek letters

α	thermal diffusivity (m^2s^{-1})
λ	dimensional viscosity variation parameter (K^{-1})
β	second-grade fluid (viscoelasticity) parameter
γ	dimensionless viscosity variation parameter
β_T	volumetric coefficient of thermal expansion (K^{-1})
Φ	viscous dissipation
ρ	density ($kg\,m^{-3}$)
$\overline{\mu}$	viscosity of the fluid ($kg\,m^{-1}s^{-1}$)
ν	kinematic viscosity (m^2s^{-1})
Ω	dimensionless temperature difference
$Br\Omega^{-1}$	dimensionless group parameter

Subscripts

l, m   grid levels in (*X, Y*) coordinate system

w   wall conditions

∞   ambient conditions

Superscript

n   time level in finite difference computation

1. INTRODUCTION

The buoyancy-induced flow [1-3] over a surface/plate and its associated fluid dynamic characteristics is of substantial interest in several industrial and engineering applications, for example, combustion flames and solar collectors, electronic equipment, building energy conservation, cooling systems, etc. Hydrodynamics and heat transfer in *non-Newtonian fluids* is also a fervent area of research due to extensive technological applications. Such fluids exhibit shear-stress-strain relationships which vary considerably from the standard Newtonian model. Many physical models have been presented to explain the diverse manner of non-Newtonian fluids. Non-Newtonian fluids include molten plastics, glues, coal in water, pulps, synthetic lubricants, polymers, ink, emulsions, etc., which feature in numerous industries, for instance, polymer processing, chemicals, pharmaceuticals, cosmetics, food stuff processing (toothpastes, jams, jellies and marmalades). Non-Newtonian fluid flow under natural convection has received significant attention by many researchers. A key early investigation of free convective heat transfer past a vertical plate for the flow of a non-Newtonian fluid was presented by Acrivos [4]. Some attempts have also been made to simulate the flow of non-Newtonian liquids with various multi-physics aspects and external to different geometrical configurations (see refs. [5-9]). Recently, Mythili et al. [10] analysed the non-Newtonian Casson fluid transport from a cone and plate in a porous medium. Among other non-Newtonian fluids, one theory that has gained prominence is the Rivlin-Ericksen theory of viscoelastic fluids. The fluids which fit this model in rheology are termed *Rivlin-Ericksen viscoelastic fluids of differential type*. This subclass of differential type fluids includes the second-grade fluid which was introduced originally by Coleman and Noll [11]. The second-grade fluid model can elegantly describe the consequences of normal stress (which may possibly lead to occurrences of 'die-swell' and 'rod-climbing', which are indexes of the stresses that develop orthogonal to planes

of shear) in polymeric flow-fields [12]. This viscoelastic fluid model shows normal stress variances in shear flow and is an approximation to simple fluids in the sense of retardation. Examples of second-grade fluid model includes, polymer melts (e.g., high-viscosity silicone oils, manufacturing oils), molten plastics (e.g. coatings), bio-technological polymers mixed in Newtonian solvents, dilute polymer solutions (e.g., polyisobutylene, polyethylene oxide in water, methyl-methacrylate in n butyl acetate, etc.). Various well-modelled multi-physical boundary value problems have been studied with second-grade viscoelastic fluid theory since the constitutive equations are slightly easier and also quite accurate estimations may be made of realistic velocity distributions. Significant modelling studies using second-grade fluid theory include thin film flow [13], magnetohydrodynamic (MHD) flows [14, 15], bio-fluid mechanics [16, 17], squeezing flow [18], and physiological hydrodynamics [19], etc. Second-grade fluid flow with heat transfer from a horizontal plate has been addressed by Kai-Long and Cheng-Hsing [20]. Pakdemirli et al. [21] studied the dynamics of non-Newtonian flow from a porous plate using a combination of the power law and second-grade fluids. Transient flow of second-grade fluid from an impulsive vertical plate was reported by Umamaheswar et al. [22]. Recently, Rahman et al. [23] investigated convective-radiative heat transfer in second-grade flow over a stretching surface.

Many of the fluids encountered in process industries, chemical and biochemical are extremely viscous in nature. The viscosity of these fluids is strongly sensitive to temperature; the thermal diffusivity, however, remains comparatively constant. Temperature-dependent fluid properties in heat transfer can significantly modify thermal/fluid characteristics [24-27]. Also, the fluid viscosity is a measure of its resistance to the flow and the temperature variation of this key hydrodynamic property should be considered. Hence robust thermo-fluid models consider the viscosity variation with thermal conditions. Some relevant studies on temperature-dependent viscosity are provided in [28-33]. Prasad et al. [34] explored the effect of temperature-dependent viscosity on magnetohydrodynamic (MHD) second-grade fluid flow with heat transfer. Thereafter, the influence of temperature dependent viscosity on viscoelastic fluid has been investigated by Faraz and Khan [35]. Second-grade fluid flow from a sheet under the effect of temperature-dependent viscosity and variable thermal conductivity was considered quite recently by Akinbobola and Samuel [36].

Thermodynamics laws are the essential principles on which all thermofluid systems are based. The first law of thermodynamics gives information regarding the energy of the system quantitatively. The second law of thermodynamics implies that entire natural processes are

irreversible and thus it is a useful approach to identify the irreversibility in any thermal system as well as to determine the optimum conditions under which the processes or devices are operated. The production of entropy measures the irreversibility in complex processes which are frequently encountered in industrial designs [37]. This methodology has therefore been successfully implemented in the various technological applications including rotating disk reactors, combustion, turbo-machinery, electronic cooling, solar energy collectors, porous media, electromagnetic materials processing and propulsion ducts. It has also been shown to achieve significant thermal efficiency improvements in power utilization, material processing, energy conservation, environmental effects, refrigeration system [38], fouling formation [39], nuclear swirl electromagnetic propulsion [40], pseudo-optimization design process modelling of solar heat exchangers [41], minimization of lost available work during process of heat transfer [42], multi-field flows [43], radiative channel flows of polar fluids for slurry systems [44] and carbon nanotube-doped cilia-assisted biomimetic propulsion [45]. Interesting recent works deploying a second law analysis include improving heat sinks in electric machines [46] and robust design in applied thermal engineering [47]. Mankind and Tsehla [48] analysed the entropy generation for nanofluid in a channel flow. Karim and John [49] studied the entropy generation for electrodialysis. Several researchers have computed the entropy heat generation for different non-Newtonian fluids and various geometries. Nagaraju et al. [50] analysed the entropy heat generation for couple stress fluid flow between two rotating cylinders. A detailed analysis of entropy generation for micropolar fluid flow through a vertical channel was conducted by Srinivas et al. [51]. Shahri and Sarhaddi [52] studied the entropy generation for two-immiscible fluids in a channel flow with nanoparticles. A number of models have also been communicated on entropy generation in the thermal transport of viscoelastic fluids. Chauhan and Kumar [53] elaborated on third-grade viscoelastic convection flow in an annulus with temperature-dependent viscosity and the second law of thermodynamics. The effect of second-grade fluid on entropy generation over a stretching plate in a porous medium was discussed by Butt et al. [54]. Recently, Rashidi *et al*. [55] analysed the entropy generation for third-grade fluid flow due to stretching sheet.

In light of the aforementioned studies, it is evident that rather limited work has been done with regard to *entropy generation minimization in unsteady second-grade fluid flow over a vertical plate*. Motivated by applications of this regime to thermal polymer processing optimization, in the present article, a computational study has been carried out for second-grade elastic-viscous natural convection flow over a semi-infinite vertical flat plate. A significant feature of

polymers is temperature-dependent viscosity. Research performed at Chevron, California in the 1960s confirmed the significant viscosity modification in many polymers with temperature [56]. Hence, temperature-dependent viscosity is taken in the current study. In this work the Crank-Nicolson implicit finite difference numerical scheme is employed to compute the non-dimensional, transient second-grade boundary layer flow problem and the solutions are validated with earlier available results from the scientific literature. The transient properties of the second-grade fluid flow with entropy heat generation are calculated for the momentum and heat transport coefficients via careful variations in a number of thermo-physical and rheological parameters (Grashof number, viscoelasticity parameter etc). Additionally, the results achieved for second-grade fluids are compared with the Newtonian fluid case. Furthermore, for the first time, an attempt is made to compute Bejan lines for the present investigated problem.

2. PROBLEM DESCRIPTION

Consider the transient two-dimensional, laminar, incompressible, buoyancy-driven flow of a second-grade viscoelastic fluid from a heated vertical plate. The plate is vertically aligned with length l and is visualized in Fig. 1. The chosen coordinate geometry is a rectangular shape, in which the x-axis and y-axis are directed vertically upward and normal to the plate, respectively. The neighbouring fluid temperature is static and analogous to that of free stream temperature T'_∞. In the beginning, i.e., $t' = 0$, the temperature T'_∞ is identical for the plate and the surrounding fluid. Later $(t' > 0)$, the temperature of the vertical plate is amplified to $T'_w \, (> T'_\infty)$ and preserved uniformly there afterward.

The Cauchy stress tensor for a second-grade differential fluid [57-58] is given by:

$$\boldsymbol{T} = -P\boldsymbol{I} + \mathrm{S} \,, \tag{1}$$

where $\mathrm{S} = \mu \mathrm{B}_1 + \alpha_1 \mathrm{B}_2 + \alpha_2 \mathrm{B}_1^2$ is the extra stress tensor. Also, $\boldsymbol{I}$, μ, P, and $\alpha'_i s \, (i = 1, 2)$ represents the identity tensor, dynamic viscosity, pressure and material constants, respectively. Further, $\mathrm{B}_1, \mathrm{B}_2$ represent the Rivlin–Ericksen tensors and are defined respectively by:

$$\mathrm{B}_1 = (\nabla \boldsymbol{q}) + (\nabla \boldsymbol{q})^{\mathrm{T}} \,,$$

$$\mathrm{B}_2 = \frac{\mathrm{dB}_1}{\mathrm{dt}} + \mathrm{B}_1(\nabla \boldsymbol{q}) + (\nabla \boldsymbol{q})^{\mathrm{T}} \mathrm{B}_1$$

in which $\frac{dB_1}{dt}$ is the material time derivative, $\boldsymbol{q}$ is the velocity and ∇ is the gradient operator.

2.1 Governing Flow-field Equations:

The mathematical model for the current problem, with the help of above definitions and assumptions, is given by the following differential equations:

(i)   Law of conservation of mass:

$$\nabla.\boldsymbol{q} = 0$$

$$\Rightarrow \quad \frac{\partial u}{\partial x} + \frac{\partial v}{\partial y} = 0 \tag{2}$$

(ii)   Law of conservation of momentum:

$$\rho\left[\frac{\partial \boldsymbol{q}}{\partial t'} + (\boldsymbol{q}.\nabla)\boldsymbol{q}\right] = \nabla.\boldsymbol{T}$$

$$\Rightarrow \quad \rho\left[\frac{\partial}{\partial t'} + u\frac{\partial}{\partial x} + v\frac{\partial}{\partial y}\right]v = -\frac{\partial p}{\partial y} + \frac{\partial}{\partial x}(S_{yx}) + \frac{\partial}{\partial y}(S_{yy})$$

$$\rho\left[\frac{\partial}{\partial t'} + u\frac{\partial}{\partial x} + v\frac{\partial}{\partial y}\right]u = -\frac{\partial p}{\partial x} + \frac{\partial}{\partial x}(S_{xx}) + \frac{\partial}{\partial y}(S_{xy})$$

in which

$$S_{yy} = \bar{\mu}\left(2\frac{\partial v}{\partial y}\right) + \alpha_1\left[\left(\frac{\partial}{\partial t'} + u\frac{\partial}{\partial x} + v\frac{\partial}{\partial y}\right)\left(2\frac{\partial v}{\partial y}\right) + 2\left\{\begin{array}{c}2\left(\frac{\partial v}{\partial y}\right)^2 + \frac{\partial u}{\partial y}\left(\frac{\partial v}{\partial x} + \frac{\partial u}{\partial y}\right) + \\ \frac{\partial w}{\partial y}\left(\frac{\partial w}{\partial y} + \frac{\partial v}{\partial z}\right)\end{array}\right\}\right] +$$

$$\alpha_2\left\{4\left(\frac{\partial v}{\partial y}\right)^2 + \left(\frac{\partial w}{\partial y} + \frac{\partial v}{\partial z}\right)^2 + \left(\frac{\partial v}{\partial x} + \frac{\partial u}{\partial y}\right)^2\right\}$$

$$S_{xx} = \bar{\mu}\left(2\frac{\partial u}{\partial x}\right) + \alpha_1\left[\left(\frac{\partial}{\partial t'} + u\frac{\partial}{\partial x} + v\frac{\partial}{\partial y}\right)\left(2\frac{\partial u}{\partial x}\right) + 2\left\{\begin{array}{c}2\left(\frac{\partial u}{\partial x}\right)^2 + \frac{\partial v}{\partial x}\left(\frac{\partial v}{\partial x} + \frac{\partial u}{\partial y}\right) + \\ \frac{\partial w}{\partial x}\left(\frac{\partial w}{\partial x} + \frac{\partial u}{\partial z}\right)\end{array}\right\}\right] +$$

$$\alpha_2\left\{4\left(\frac{\partial u}{\partial x}\right)^2 + \left(\frac{\partial w}{\partial x} + \frac{\partial u}{\partial z}\right)^2 + \left(\frac{\partial v}{\partial x} + \frac{\partial u}{\partial y}\right)^2\right\}$$

$$S_{xy} = S_{yx} = \bar{\mu}\left(\frac{\partial u}{\partial y} + \frac{\partial v}{\partial x}\right) + \alpha_1\left[\begin{array}{c}\left(\frac{\partial}{\partial t'} + u\frac{\partial}{\partial x} + v\frac{\partial}{\partial y}\right)\left(\frac{\partial u}{\partial y} + \frac{\partial v}{\partial x}\right) + 2\frac{\partial u}{\partial y}\frac{\partial u}{\partial x} + \frac{\partial v}{\partial y}\left(\frac{\partial u}{\partial y} + \frac{\partial v}{\partial x}\right) \\ +2\frac{\partial v}{\partial y}\frac{\partial v}{\partial x} + \frac{\partial w}{\partial y}\left(\frac{\partial u}{\partial z} + \frac{\partial w}{\partial x}\right) + \frac{\partial u}{\partial x}\left(\frac{\partial u}{\partial y} + \frac{\partial v}{\partial x}\right) + \frac{\partial w}{\partial x}\left(\frac{\partial v}{\partial z} + \frac{\partial w}{\partial y}\right)\end{array}\right] +$$

$$\alpha_2\left\{2\frac{\partial u}{\partial x}\left(\frac{\partial u}{\partial y} + \frac{\partial v}{\partial x}\right) + \left(\frac{\partial u}{\partial z} + \frac{\partial w}{\partial x}\right)\left(\frac{\partial v}{\partial z} + \frac{\partial w}{\partial y}\right) + 2\frac{\partial v}{\partial y}\left(\frac{\partial v}{\partial x} + \frac{\partial u}{\partial y}\right)\right\}$$

where u and v signify the velocity components along the axial (x) and transverse (y) directions, respectively, ρ is the density and S_{xx}, S_{xy}, S_{yx}, S_{yy} are the extra stress components.

The Clausius-Duhem inequality and the condition that the Helmholtz free energy is minimum at equilibrium hold provided the following conditions [59] are satisfied.

$$\bar{\mu} \geq 0, \ \ \alpha_1 \geq 0, \ \ \alpha_1 + \alpha_2 = 0. \tag{3}$$

The flow is presumed to be along the axial direction only and hence by ignoring the transverse direction, the governing unsteady boundary layer equations for momentum and heat conservation of the second-grade fluid with the above inequality and restrictions in Eqn. (3) and using Boussinesq's approximation are as follows:

$$\frac{\partial u}{\partial t'} + u\frac{\partial u}{\partial x} + v\frac{\partial u}{\partial y} = \ g\beta_T(T' - T'_\infty) + \frac{1}{\rho}\frac{\partial}{\partial y}\left(\bar{\mu}\frac{\partial u}{\partial y}\right)$$

$$+\frac{\alpha_1}{\rho}\left(\frac{\partial^3 u}{\partial y^2 \partial t'} + \frac{\partial u}{\partial x}\frac{\partial^2 u}{\partial y^2} + u\frac{\partial^3 u}{\partial x \partial y^2} + v\frac{\partial^3 u}{\partial y^3} - \frac{\partial u}{\partial y}\frac{\partial^2 v}{\partial y^2}\right) \tag{4}$$

(iii)   Law of conservation of energy:

$$\left[\frac{\partial T'}{\partial t'} + (\boldsymbol{q}.\nabla)T'\right] = \alpha(\nabla^2 T')$$

$$\Rightarrow \qquad \frac{\partial T'}{\partial t'} + u\frac{\partial T'}{\partial x} + v\frac{\partial T'}{\partial y} = \alpha\frac{\partial^2 T'}{\partial y^2} \tag{5}$$

The associated initial and boundary conditions are given by:

$$t' \leq 0: \ \ T' = T'_\infty, u = 0, v = 0 \qquad\qquad \text{for all } x \text{ and } y$$

$$t' > 0: \ \ T' = T'_w, \ \ u = 0, v = 0 \qquad\qquad \text{at } y = 0$$

$$T' = T'_\infty, \ \ u = 0, v = 0 \qquad\qquad \text{at } x = 0 \tag{6}$$

$$T' \to T'_\infty, u \to 0, \frac{\partial u}{\partial y} \to 0, v \to 0 \qquad \text{as } y \to \infty$$

We invoke the following non-dimensional quantities (for all symbols refer to the nomenclature):

$$X = \text{Gr}^{-1}\frac{x}{l}, \ Y = \frac{y}{l}, U = \text{Gr}^{-1}\frac{ul}{v}, \ V = \frac{vl}{v}, \ \ t = \frac{vt'}{l^2}, T = \frac{T'-T'_\infty}{T'_w-T'_\infty}, Gr = \frac{g\beta_T l^3\left(T'_w-T'_\infty\right)}{v^2},$$

$$Pr = \frac{v}{\alpha}, v = \frac{\mu_\infty}{\rho}, Br = \frac{\mu v^2}{k(T'_w-T'_\infty)l^2}, \ \Omega = \frac{(T'_w-T'_\infty)}{T'_\infty}, \beta = \alpha_1/\rho l^2$$

The viscosity variation with temperature is analysed by the robust models developed and applied by Ling and Dybbs [25] and Molla et al. [26]:

$$\overline{\mu}(T') \cong \frac{\mu_\infty}{\left(1+b\left(T'-T'_\infty\right)\right)}$$

where $\overline{\mu}$ is the viscosity of the fluid depending on temperature T', b is a constant and μ_∞ denotes fluid dynamic viscosity at the temperature T'_∞. Let γ signifies the dimensionless viscosity variation parameter and is given by $\gamma = b(T'_w - T'_\infty)$. It follows that the fluid viscosity in non-dimensional temperature can be written as

$$\overline{\mu}(T) = \frac{\mu_\infty}{(1+\gamma T)} \tag{7}$$

Incorporating the above cited dimensionless numbers in Eqns. (2), (4), (5) and also in Eqn. (6), the conservations equations contract to the following:

$$\frac{\partial U}{\partial X} + \frac{\partial V}{\partial Y} = 0 \tag{8}$$

$$\frac{\partial U}{\partial t} + U\frac{\partial U}{\partial X} + V\frac{\partial U}{\partial Y} = T + \frac{1}{(1+\gamma T)}\frac{\partial^2 U}{\partial Y^2} - \frac{\gamma}{(1+\gamma T)^2}\frac{\partial T}{\partial Y}\frac{\partial U}{\partial Y}$$

$$+\beta\left(\frac{\partial^3 U}{\partial Y^2 \partial t} + \frac{\partial U}{\partial X}\frac{\partial^2 U}{\partial Y^2} + U\frac{\partial^3 U}{\partial X \partial Y^2} + V\frac{\partial^3 U}{\partial Y^3} - \frac{\partial U}{\partial Y}\frac{\partial^2 V}{\partial Y^2}\right) \tag{9}$$

$$\frac{\partial T}{\partial t} + U\frac{\partial T}{\partial X} + V\frac{\partial T}{\partial Y} = \frac{1}{Pr}\frac{\partial^2 T}{\partial Y^2} \tag{10}$$

$$
\begin{aligned}
t \leq 0: \quad & T = 0, \; U = 0, \; V = 0 && \text{for all } X \text{ and } Y \\
t > 0: \quad & T = 1, \; U = 0, \; V = 0 && \text{at } Y = 0 \\
& T = 0, \; U = 0, V = 0 && \text{at } X = 0 \\
& T \to 0, U \to 0, \frac{\partial U}{\partial Y} \to 0, V \to 0 && \text{as } Y \to \infty
\end{aligned}
\tag{11}
$$

3. FINITE DIFFERENCE NUMERICAL SOLUTION

To solve the nonlinear time-dependent governing Eqns. (8) - (10) together with initial and boundary conditions (11), a stable (unconditionally) implicit scheme "Crank-Nicolson method" is applied. This implicit scheme remains very versatile in unsteady heat transfer and fluid dynamics. It has been employed in viscoelastic flows by Prasad *et al.* [60] for unsteady flat plate free convection flows. An excellent description of the Crank-Nicolson method in the

context of natural convection flows is provided in Cebeci [61]. Let $A = \dfrac{1}{1+\lambda\left(\frac{T_{l,m}^{n+1}+T_{l,m}^{n}}{2}\right)}$, then the

finite difference equations corresponding to the above Eqns. (8)-(10) take the form:

$$\frac{U_{l,m}^{n+1}-U_{l-1,m}^{n+1}+U_{l,m}^{n}-U_{l-1,m}^{n}}{2\Delta X} + \frac{V_{l,m}^{n+1}-V_{l,m-1}^{n+1}+V_{l,m}^{n}-V_{l,m-1}^{n}}{2\Delta Y} = 0 \tag{12}$$

$$\frac{U_{l,m}^{n+1}-U_{l,m}^{n}}{\Delta t}+\frac{U_{l,m}^{n}}{2\Delta X}\left(U_{i,j}^{k+1} - U_{i-1,j}^{k+1} + U_{i,j}^{k} - U_{i-1,j}^{k}\right)+\frac{V_{i,j}^{k}}{4\Delta Y}\left(U_{l,m+1}^{n+1} - U_{l,m-1}^{n+1} + U_{l,m+1}^{n} - U_{l,m-1}^{n}\right)$$

$$= \frac{T_{l,m}^{n+1}+T_{l,m}^{n}}{2} + A\left(\frac{U_{l,m+1}^{n+1}-2U_{l,m}^{n+1}+U_{l,m-1}^{n+1}+U_{l,m+1}^{n}-2U_{l,m}^{n}+U_{l,m-1}^{n}}{2(\Delta Y)^2}\right)$$

$$-\lambda A^2\left(\frac{T_{l,m+1}^{n+1}-T_{l,m-1}^{n+1}+T_{l,m+1}^{n}-T_{l,m-1}^{n}}{4(\Delta Y)}\right)\left(\frac{U_{l,m+1}^{n+1}-U_{l,m-1}^{n+1}+U_{l,m+1}^{n}-U_{l,m-1}^{n}}{4(\Delta Y)}\right)$$

$$+\beta\left[\frac{U_{l,m+2}^{n+1}-2U_{l,m}^{n+1}+U_{l,m-2}^{n+1}-U_{l,m+2}^{n}+2U_{l,m}^{n}-U_{l,m-2}^{n}}{4(\Delta Y)^2\Delta t}\right]$$

$$+\beta U_{l,m}^{n}\left[\frac{U_{l,m+1}^{n+1}-U_{l-1,m+1}^{n+1}-2U_{l,m}^{n+1}+2U_{l-1,m}^{n+1}+U_{l,m-1}^{n+1}-U_{l-1,m-1}^{n+1}+U_{l,m+1}^{n}-U_{l-1,m+1}^{n}-2U_{l,m}^{n}+2U_{l-1,m}^{n}+U_{l,m-1}^{n}-U_{l-1,m-1}^{n}}{2(\Delta Y)^2\Delta X}\right]$$

$$+\beta V_{l,m}^{n}\left[\frac{\left(U_{l,m+2}^{n+1}-2U_{l,m+1}^{n+1}+2U_{l,m-1}^{n+1}+U_{l,m-2}^{n+1}+U_{l,m+2}^{n}-2U_{l,m+1}^{n}+2U_{l,m-1}^{n}+U_{l,m-2}^{n}\right)}{4(\Delta Y)^3}\right]$$

$$+\beta\left[\frac{U_{l,m}^{n}-U_{l-1,m}^{n}}{\Delta X}\right]\left[\frac{U_{l,m+1}^{n+1}-2U_{l,m}^{n+1}+U_{l,m-1}^{n+1}+U_{l,m+1}^{n}-2U_{l,m}^{n}+U_{l,m-1}^{n}}{2(\Delta Y)^2}\right]$$

$$-\beta\left[\frac{U_{l,m}^{n}-U_{l,m-1}^{n}}{\Delta Y}\right]\left[\frac{V_{l,m+1}^{n+1}-2V_{l,m}^{n+1}+V_{l,m-1}^{n+1}+V_{l,m+1}^{n}-2V_{l,m}^{n}+V_{l,m-1}^{n}}{2(\Delta Y)^2}\right]$$

$$-\beta\left[\frac{U_{l,m+1}^{n}-2U_{l,m}^{n}+U_{l,m-1}^{n}}{(\Delta Y)^2}\right]\left[\frac{U_{l,m+1}^{n+1}-U_{l,m-1}^{n+1}+U_{l,m+1}^{n}-U_{l,m-1}^{n}}{4(\Delta Y)}\right] \tag{13}$$

$$\frac{T_{l,m}^{n+1}-T_{l,m}^{n}}{\Delta t}+\frac{U_{l,m}^{n}}{2\Delta X}\left(T_{l,m}^{n+1} - T_{l-1,m}^{n+1} + T_{l,m}^{n} - T_{l-1,m}^{n}\right)+\frac{V_{l,m}^{n}}{4\Delta Y}\left(T_{l,m+1}^{n+1} - T_{l,m-1}^{n+1} + T_{l,m+1}^{n} - T_{l,m-1}^{n}\right)$$

$$= \left[\frac{T_{l,m+1}^{n+1}-2T_{l,m}^{n+1}+T_{l,m-1}^{n+1}+T_{l,m+1}^{n}-2T_{l,m}^{n}+T_{l,m-1}^{n}}{2Pr(\Delta Y)^2}\right] \tag{14}$$

In the above equations (12), (13) and (14), l and m are the subscripts which represent the mesh points along the X and Y coordinates, respectively, where $X = l\Delta X$ and $Y = m\Delta Y$ and the superscript n describes a value of the time $t(= n\Delta t)$ with ΔX, ΔY and Δt the grid sizes in the X, Y and t axes, respectively. The numerical equations are solved on the rectangular grid with $X_{max} = 1$, $X_{min} = 0$, $Y_{max} = 20$ and $Y_{min} = 0$, where Y_{max} relates to $Y = \infty$ which lies far away from the heat and momentum transport boundary layers.

4. GRID (MESH) INDEPENDENCE STUDY

To obtain an efficient consistent grid (mesh) system for the numerical simulations, a grid independency test is performed for different mesh sizes of 25 X 125, 50 X 250, 100 X 500 and 200 X 1000 and the values of the $\overline{Nu}$ on the boundary $Y = 0$ corresponding to each of these grids are documented in Table 1. It is noticed from Table 1 that 100 X 500 (grid size) compared with 50 X 250 and 200 X 1000 (grid sizes) does not incur any significant modification on the results of average heat transport coefficient. Thus, 100 X 500 (grid size) is demonstrably adequate for this problem with the step sizes of 0.01 and 0.04 in axial and transverse directions, respectively. Similarly, in order to produce reliable results with respect to time, a grid-independence test has been performed for different time step sizes, as shown in Table 2. The effective selected time step size Δt ($t = n\Delta t, n = 0, 1, 2, ...$) is fixed as 0.01.

The finite difference technique starts by computing the solution for the thermal boundary layer Eqn. (14), which provides the *temperature field*. Next solving the conservation of momentum and mass Eqns. (13) and (12) provides the solution for the velocity field. Eqns. (13) - (14) at the $(n{+}1)^{\text{th}}$ stage are stated in the following tri-diagonal and penta-diagonal forms:

$$a_{l,m}\Omega_{l,m-1}^{n+1} + b_{l,m}\Omega_{l,m}^{n+1} + c_{l,m}\Omega_{l,m+1}^{n+1} = d_{l,m}^{n},$$

$$A_{l,m}\omega_{l,m-2}^{n+1} + B_{l,m}\omega_{l,m-1}^{n+1} + C_{l,m}\omega_{l,m}^{n+1} + D_{l,m}\omega_{l,m+1}^{n+1} + E_{l,m}\omega_{l,m+2}^{n+1} = F_{l,m}^{n}, \qquad (15)$$

Here Ω and ω indicates the transient flow-field variables *T* and *U*. Thus, Eqns. (13) -(14) at each interior grid point on a precise *l*-level comprise a system of tri-diagonal and penta-diagonal equations. Further detailed descriptions of this finite difference method can be found in the available literature [62].

5. RESULTS AND DISCUSSION

To analyse the transient nature of the flow-field profiles, such as velocity and temperature, their values are shown at various locations which are adjacent to the vertical plate.

The computed flow-field variables for the case of Newtonian fluids ($\beta = 0.0$) are related with those of Takhar et al. [63] for $Pr = 0.7, \gamma = 0$, and are shown in Fig. 2. The numerical

values are found to be in good agreement. This confirms the accuracy and validity of the existing numerical scheme. Variation of simulated flow-field variables is plotted with different control parameter values such as second-grade fluid parameter (β), viscosity variation parameter (γ), Grashof number (*Gr*), group parameter ($Br\Omega^{-1}$) and Prandtl number (*Pr*) in subsequent Figures.

The result of choosing viscosity variation parameter (γ) given in the Eqn. (7). If γ < 0, then $\overline{\mu}(T)$ is large, the influence of variable viscosity can be neglected. If γ ≥ 0, then $\overline{\mu}(T)$ is small, and the effect of variable viscosity is taken into consideration.

The range of second grade fluid parameter β is chosen from the following definition (β = $\alpha_1/\rho l^2$) (Dunn and Rajagopal [59]), in which α_1 is the normal stress moduli. If α_1 is positive, the model has a good behaviour in the sense that stability and unboundedness may be achieved, whereas if $\alpha_1$is taken to be negative, then in quite arbitrary flows, instability and boundedness are unavoidable. Therefore, they have concluded that the only second grade fluid to be found in nature is one with β ≥ 0.

The Grashof number states the ratio between the buoyancy force and the viscous force. When *Gr* is high, the viscous force is negligible as compared to the buoyancy and inertial forces. When buoyant forces overcome the viscous forces, the flow starts a transition to the turbulent regime. Furthermore, at smaller values of Grashof number the induced flow moves upward making a smooth turn around the hot vertical plate.

5.1 Velocity and Temperature Variables

In this sub-section, the effects of dimensionless physical parameters on the velocity components are analysed, based on Figs. 3-4. Figure 3 depicts the variation of simulated transient velocity (*U*) versus time (*t*) at the position (0, 1.56) for distinct values of viscosity variation parameter (γ) and viscoelastic parameter (*β*). At all locations, the velocity curve augments with time, attain the temporal maxima, then slightly decrease, and finally, they turn out to be independent of time. The non-linear characteristics of the unsteady momentum equation in consistency with certain values of non-dimensional viscosity $1/(1 + \gamma T)$ and non-dimensional thermal diffusivity $1/Pr$ are probably the cause of the velocity overshoot. The time-dependent *U* profile initially upturns with increasing γ. With increasing γ the size of the velocity term reduced (refer to Eq. (9)) which produces less resistance to the fluid flow in the region of the temporal peak velocities. Also, fluid viscosity is decreased with greater γ and this reduces viscous forces in the boundary layer which accelerates the flow. With rising values of

viscoelasticity parameter, β the flow is decelerated since greater elastic effects are induced as per the definition of this parameter ($= \frac{\alpha_1}{\rho l^2}$). This energizes the flow and assists momentum development.

Figure 4 illustrates the time-independent state velocity curves for different control parameters (β and γ) against Y coordinate. It is perceived that the U curves in this figure begin with the no-slip boundary condition, attains its peak and then drops to zero along the Y coordinate satisfying the outlying boundary conditions. In the environs of the hot vertical plate, the magnitude of dimensionless axial velocity (U) is amplified with greater Y values, attaining a peak close to the wall into the boundary layer. Further, the time taken to reach the steady-state condition reduces as γ increases while the reverse trend is seen for β. Additionally, it is apparent that in the vicinity of the hot wall the velocity magnitude is high for γ compared to β since viscosity decreasing with increasing γ, i.e. γ have a more profound accelerating influence on axial velocity.

Figure 5 describes the effect of γ and β on transient temperature profile (T) against time (t) at the spatial location (0, 0.68). From this graph, initially, temperature is accentuated with t, attains a maximum and thereafter is weakly decreased, finally attaining the time independent-state. Temperature is reduced with greater values of γ. This is due to the fact that as γ increases the viscosity of the fluid decreases [refer to Eqn. (7)] which allows leads to a decrease also in thermal diffusion and plummet in temperature profiles. Also, for escalating β, temperature is clearly increased. The upsurge in the temperature of the fluid is attributable to stronger elastic forces in the medium and also a modification in viscosity which enhances motion of the fluid. For all transient T profiles, asymptotically smooth declines are seen in the free stream confirming the imposition of an adequately large infinity boundary condition in the Crank-Nicolson numerical code.

Figure 6 depicts the time-independent T profiles versus transverse coordinate (Y) for different values of γ and β. These outlines originate with the boundary value of $T = 1$ and then decrease to zero. It is well-known that, as γ increases, the temperature decreases. Also enhancing β eventually results in a boost in temperature as revealed in Fig. 6. Also, it is noted that the time-independent state T profiles have coincided with each other for various values of γ and β as Y increases from 0 to 3. Hence, the influence of γ or β on T profiles have less impact related to the U profiles as revealed in Fig. 4. This is logical since the physical parameters γ

and β appear only in the momentum equation (9) and therefore the dominant influence is on velocity.

5.2 Friction and Heat Transport Coefficients

From the thermal engineering view point the wall shear-stress and heat transfer rate quantities are significant design parameters. This is also the case for a non-Newtonian fluid (second-grade fluid), since these design quantities are substantially influenced by the natural convection process. For the current second-grade fluid flow problem, the dimensionless *average momentum and heat transfer coefficients* are defined as:

$$\overline{C_f} = \frac{1}{(1+\gamma)} \int_0^1 \left(\frac{\partial U}{\partial Y}\right)_{Y=0} dX \tag{16}$$

$$\overline{Nu} = - \int_0^1 \left(\frac{\partial T}{\partial Y}\right)_{Y=0} dX \tag{17}$$

The above coefficients are evaluated using 5-point approximation and Newton–Cotes quadrature formulae.

Figures 7-8 illustrate transient $\overline{C_f}$ and $\overline{Nu}$ profiles against time (t) of second-grade fluid flow for a variation in the parameters, γ and β. Figure 7 shows that, in the beginning, $\overline{C_f}$ upsurges with time t and later a certain interval of time it achieves the steady-state magnitude. There is a significant decrease in $\overline{C_f}$ with viscosity parameter (γ) owing to the deceleration in the flow with greater viscosity effects. This trend is similar to that of the time-dependent velocity profile computed in Fig. 3. Also, rising values of β manifest in a marked reduction in $\overline{C_f}$ $i.\,e.$ a strong deceleration at the wall is induced with stronger viscoelastic effects.

Figure 8 demonstrates that initially, $\overline{Nu}$ declines significantly, a trend which is followed by a slight increase in magnitudes and subsequent attainment of the steady-state. Moreover, it is observed that initially, the $\overline{Nu}$ curves of second-grade fluid coincide with each other and they deviate after some time interval. These figures designate that at the initiation of the buoyancy-driven flow, thermal conduction heat transfer dominates over convection; only with progression in time are the free convection currents mobilized. Also, it is also evident that $\overline{Nu}$ upsurges with increasing values of γ which are physically reliable with an upsurge in

temperatures in the boundary layer (computed earlier). Whereas for enhancing β, the $\overline{Nu}$ shows decreasing trend.

5.3 Entropy Heat Generation Analysis and Bejan Number Computation

The entropy generation for a second-grade fluid per unit volume with constant density is given by the following expression:

$$S_{gen} = \frac{k}{T_\infty'^2}(\nabla T')^2 + \frac{1}{T_\infty'}\Phi$$

$$\Rightarrow \qquad S_{gen} = \frac{k}{T_\infty'^2}\left(\frac{\partial T'}{\partial y}\right)^2 + \left\{\frac{\bar{\mu}}{T_\infty'}\left(\frac{\partial u}{\partial y}\right)^2 + \frac{\alpha_1}{T_\infty'}\left[\frac{\partial^2 u}{\partial y \partial t'}\frac{\partial u}{\partial y} + v\frac{\partial u}{\partial y}\frac{\partial^2 u}{\partial y^2} + u\frac{\partial u}{\partial y}\frac{\partial^2 u}{\partial x \partial y}\right]\right\} \qquad (18)$$

The equation (18) can be rewritten as

$$S_{gen} = S_1 + S_2$$

where $\quad S_1 = \frac{k}{T_\infty'^2}\left(\frac{\partial T'}{\partial y}\right)^2,$

$$S_2 = \frac{\bar{\mu}}{T_\infty'}\left(\frac{\partial u}{\partial y}\right)^2 + \frac{\alpha_1}{T_\infty'}\left[\frac{\partial^2 u}{\partial y \partial t'}\frac{\partial u}{\partial y} + v\frac{\partial u}{\partial y}\frac{\partial^2 u}{\partial y^2} + u\frac{\partial u}{\partial y}\frac{\partial^2 u}{\partial x \partial y}\right].$$

Here S_1 indicates the entropy generation due to heat flow, S_2 represents the entropy generation due to viscous dissipation.

The dimensionless entropy heat generation parameter *Ns* is defined as the ratio of the volumetric entropy heat generation rate to the characteristic entropy heat generation rate [64]. Thus, the entropy generation number for the current problem can be written as:

$$N_S = \left(\frac{\partial T}{\partial Y}\right)^2 + \frac{Br(Gr)^2}{\Omega}\left\{\frac{1}{(1+\gamma T)}\left(\frac{\partial U}{\partial Y}\right)^2 + \beta\left(\frac{\partial^2 U}{\partial Y \partial t}\frac{\partial U}{\partial Y} + V\frac{\partial U}{\partial Y}\frac{\partial^2 U}{\partial Y^2} + U\frac{\partial U}{\partial Y}\frac{\partial^2 U}{\partial X \partial Y}\right)\right\} \qquad (19)$$

where $\Omega = \frac{(T_w' - T_\infty')}{T_\infty'}$ is the dimensionless temperature difference, and the characteristic entropy heat generation is $\frac{k(T_w' - T_\infty')^2}{T_\infty'^2 l^2}$. Eqn. (19) can be rewritten in the following compact form

$$N_S = N_1 + N_2 \qquad (20)$$

Here the following definitions apply:

$$N_1 = \left(\frac{\partial T}{\partial Y}\right)^2 \text{ and } N_2 = \frac{Br(Gr)^2}{\Omega}\left\{\frac{1}{(1+\gamma T)}\left(\frac{\partial U}{\partial Y}\right)^2 + \beta\left(\frac{\partial^2 U}{\partial Y \partial t}\frac{\partial U}{\partial Y} + V\frac{\partial U}{\partial Y}\frac{\partial^2 U}{\partial Y^2} + U\frac{\partial U}{\partial Y}\frac{\partial^2 U}{\partial X \partial Y}\right)\right\} \qquad (21)$$

N_1 and N_2 describe the irreversibility due to heat transfer and fluid friction (viscous dissipation), respectively.

To evaluate the irreversibility distribution, the parameter *Be* (Bejan number) is utilized and this is defined as the ratio of entropy heat generation due to heat transfer to the overall entropy heat production and is given by

$$Be = \frac{N_1}{N_1 + N_2} \tag{22}$$

From the Eq. (22), it is clear that the range of Bejan number is from 0 to 1 i.e. $0 \leq Be \leq 1$. Subsequently, $Be = 0$ reveals that the N_2 parameter dominates the N_1 parameter, whereas $Be = 1$ designates that the N_1 parameter dominates the N_2 parameter. It is observable that at $Be = 0.5$, the contribution of fluid friction in the entropy generation production is the same as heat transfer irreversibility, i.e. $N_2 = N_1$.

The effect of the various physical parameters on entropy heat generation (*Ns*) distribution against time (*t*) at the spatial location (0, 0.76) is depicted in Fig. 9. The influence of viscosity variation parameter (γ), the second-grade fluid parameter (β), group parameter ($Br\Omega^{-1}$) and Grashof number (*Gr*) on the unsteady distribution of *Ns* are shown in Figs. 9(a) – 9(b), respectively. From all these graph, it is find out that, in the beginning, the *Ns* curves upsurges drastically, then decreases, again upsurges, attains the temporal peak, and towards the end it emerges that it is independent of time. The significant observation to be made from these transient graphs is that, in the initial time stage, all *Ns* curves are combined and split later for all values of physical parameters. This specifies that at preliminary time levels (i.e., $t < 6$) thermal conduction is dominant over the thermal convection heat transfer. Later, after a certain elapse of time, the rate of heat-transfer is dominated by the influence of free convection with escalating entropy production. Before attainment of the steady-state, overshoots of the entropy generation profile occur. From Fig. 9(a), it is seen that the *Ns* increase with increasing γ. Whereas reverse trend is observed for the viscoelastic parameter. In the Fig. 9(b), the *Ns* curves follow the similar transient tendency as described in the Fig. 9(a). Thus, from the Fig. 9(b) is noted that intensifying the values of flow-field parameter results in high entropy production, especially with increasing group parameter, $Br\Omega^{-1}$. With greater values of this composite parameter, entropy generation due to the fluid friction is boosted in the regime.

The computer-generated steady-state entropy curves for various control parameters γ, β, $Br\Omega^{-1}$ and *Gr* against *Y* at *X* = 1.0 are shown in Figures 10(a)-10(b), respectively. Here, it is

seen that as the transverse coordinate rises, the *Ns* magnitudes noticeably increase and achieve their maximum magnitudes, then decrease swiftly and decay to zero. Also, it is apparent that the entropy production acquires thinner boundary layer for all values of physical parameters. This is as a consequence of greater production of entropy which is generated in close proximity to the plate which produces a thinner boundary layer. Figure 10(a) depicts the variation of γ and β on *Ns*. From this graph, it is apparent that in the neighbourhood of the hot plate (i.e., in the interval $Y \in [0, 1.2]$) the steady-state *Ns* curves increases for augmenting values of γ and decreases for rising values of β. Whereas the trend is reversed when $Y > 1.2$. Figure 10(b) signifies that the entropy rises in the vicinity of the hot plate then drops and approaches to zero along the *Y* coordinate. Also, it is noted that with greater values of $Br\Omega^{-1}$ and *Gr*, the *Ns* curves upsurge considerably, since for higher values of the group parameter or Grashof number, the entropy production owing to the fluid friction is enhanced.

Figures 11(a) – 11(b) illustrate the evolution of Bejan number (*Be*) with time (*t*) at $Y = 0.76$ and $X = 1.0$, for various values of physical parameters. The patterns indicate that at commencement of the flow, *Be* has zero value, upsurges slightly with *t*, then decreases negatively in the interval of time $t \in (2.4, 4.6)$, rises drastically and reaches the maximum value, then falls marginally, and lastly exhibits no tangible dependence on time. At the initiation of the thermal convection flow, the irreversibility caused by heat transfer regulates the entropy and when $t > 5$, the fluid friction dominates. From Fig. 11(a) in the main, it is apparent that as γ increases the Bejan number reduces. Also, it is evident that increasing β causes an enhancing value in *Be*. From the Fig. 11(b) it is clear that as $Br\Omega^{-1}$ or *Gr* increases, the Bejan number increases i.e. *viscous heating and thermal buoyancy both enhance Bejan number.*

Lastly, Fig. 12 shows the steady-state *Be* against the transverse coordinate (*Y*) for different parameter values. The influence of γ, β, $Br\Omega^{-1}$ and *Gr* on *Be* are revealed in Figs. 12(a)-12(b), respectively. From all these plots, it is observed that the time-independent state features of Bejan number are quite different from that of steady state entropy generation (*Ns*) which is revealed in the Figs. 10(a) – 10(b). In particular, it may be deduced that, irreversibility owing to heat transfer arises in the transverse coordinate interval, i.e., $Y \in (1.2, 1.8)$ which accounts for the negative values in *Be*. Generally, it is noted from Fig. 12(a), that the steady-state *Be* upsurges for an increase in the values of all physical parameters. Also, inspection of Fig. 12(b) reveals that *Be* is boosted with greater values of $Br\Omega^{-1}$ and *Gr*. The significant implication

from these graphs is that the steady-state entropy production exceeds the Bejan number adjacent to the wall. This verifies that smaller *Be* produces an escalation in N_2, i.e., $N_1 < N_2$ (Refer Eq. 22) and thus irreversibility due to heat transfer is dominated by fluid friction which manifests in intensified entropy production in the neighbourhood of the hot wall.

Figures 13(a)-13(d) present the entropy lines for various parameter values (γ, β, $Br\Omega^{-1}$ and *Gr*). In all these graphs, it is seen that the entropy lines rise in the vicinity of the hot plate for all values of physical parameters. From Figs. 13(a)-13(b) it is also noticed that at any point of position (X, Y) the entropy contour value upsurges for augmenting values of γ and decreases for augmenting values of β. A similar tendency is observed for values of $Br\Omega^{-1}$ and *Gr* which is shown in Figs.13(c)-13(d). It is perceived that in the two-dimensional rectangular coordinate system i.e. $0 < X \leq 1, 0, \ 0 < Y \leq 0.5$, the entropy lines fluctuate with a change in the values of $Br\Omega^{-1}$ and *Gr* as compared to γ and β. Also, nearby the forefront of the vertical plate the entropy contours show higher values for γ, $Br\Omega^{-1}$ and *Gr* as compared to β. This is attributable to the fact that the entropy production is high for γ, $Br\Omega^{-1}$ and *Gr* near to the boundary layer leading edge of the plate as compared to β.

Figures 14(a)-14(d) visualize the Bejan lines for various values of γ, β, $Br\Omega^{-1}$ and *Gr*, respectively. In all these graphs, the Bejan lines show a unique trend for all physical parameters as compared to entropy lines which are shown in Figs. 13(a) -13(d). Further, in the proximity of the hot plate it is well-known that Bejan lines are inclined to move away from the plate with increase in the physical parameters γ and β as *Y* increases, whereas these lines tend to adhere to the plate with modification in the values of $Br\Omega^{-1}$ and *Gr*. Also, it is noteworthy that the Bejan lines occur only in the region close to the hot vertical plate.

5.4 Comparison between Second-grade Viscoelastic and Newtonian Fluid Flows

Figure 15 reveals the flow-field variable contours for the second-grade and Newtonian fluid flows. Fig. 15(a) represents the Newtonian fluid case and Fig. 15(b) corresponds to the second-grade fluid. The velocity of the second-grade fluid flow is found to be lower compared to that of the Newtonian fluid flow; however, with regard to the temperature distribution, the reverse trend is noticed. Furthermore, the steady-state temperature contours for the second-grade fluid are somewhat different and a thicker thermal boundary layer is achieved compared with the Newtonian fluid.

6. CONCLUDING REMARKS

In the present research article, the heat transfer and entropy generation distributions for time-dependent second-grade fluid from a semi-infinite vertical plate with viscosity variation have been studied numerically. A Crank-Nicolson finite difference method is applied to solve the normalized mass, momentum, and energy conservation boundary layer equations under appropriate initial and boundary conditions with the help of Thomas and penta-diagonal algorithms. The entropy generation and Bejan numbers are derived and evaluated with the help of flow variables. Velocity, temperature, average momentum (skin friction) and heat transport (Nusselt number) coefficients are computed and displayed graphically. The effects of viscosity variation parameter, viscoelastic parameter, Brinkman combined parameter and Grashof number on these thermal/flow characteristics in addition to entropy generation number and Bejan number are evaluated. The salient conclusions from the current study may be summarized as follows:

1. The velocity is enhanced whereas the temperature decreases with rising values of γ and the converse response are observed with an increase β.

2. The time taken to attain the time-independent state decreases as temperature-dependent viscosity (γ) is increased, and the opposite behaviour is induced with increasing viscoelastic parameter (β).

3. Average wall shear stress ($\overline{C_f}$) and wall heat transfer rate ($\overline{Nu}$) are reduced with augmenting values of viscoelastic parameter (β).

4. Entropy heat generation number is reduced with greater values of viscoelastic parameter (β). The reverse trend is induced by increasing viscosity variation parameter, Brinkman combined group parameter and Grashof number (thermal buoyancy parameter).

5. Bejan number is elevated with a rise in the values of all the thermophysical or rheological parameters except the viscosity variation parameter, γ.

important areas for improvement in this article. Their suggestions have served in particular, to enhance the clarity and depth of the interpretation.

REFERENCES

1. Gnaneswara Reddy, M and Bhaskar Reddy, N. Unsteady MHD convective heat and mass Transfer past a semi-infinite vertical porous plate with variable viscosity and thermal conductivity, *Int. J. Appl. Math. Comp.*, **1**, 104-117 (2009).

2. Gnaneswara Reddy, M. Unsteady heat and mass transfer mhd flow of a chemically reacting fluid past an impulsively started vertical plate with radiation, *J. Eng. Phy. Therm.*, 87, 1233-1240 (2014).

3. Gnaneswara Reddy, M and Sandeep, N. Computational modelling and analysis of heat and mass transfer in MHD flow past the upper part of a paraboloid of revolution, Eur. Phys. J. Plus, **132**, 1-18 (2017).

4. Acrivos, A. A Theoretical analysis of laminar natural convection heat transfer to non-Newtonian fluids, A.1.Ch.E. J., **4**, 584-590 (1960).

5. Chen, HT. and Chen, CH. Free convection flow of non-Newtonian fluids along a vertical plate embedded in a porous medium, *J. Heat Transf*. **110**, 257-260 (1988).

6. Gnaneswara Reddy, M. Unsteady radiative - convective boundary-layer flow of a Casson fluid with variable thermal conductivity, *J. Eng. Phy. Therm*. **88**, 240-251 (2015).

7. Prakash, D and Muthtamilselvan, M. Effect of radiation on transient MHD flow of micropolar fluid between porous vertical channel with boundary conditions of the third kind, *Ain Shams Eng. J.* **5**, 1277-1286 (2014).

8. Gnaneswara Reddy, M. Cattaneo-Christov heat flux effect on hydromagnetic radiative Oldroyd-B liquid flow across a cone/wedge in the presence of cross-diffusion, *Eur. Phys. J. Plus.* **133**, 1-18 (2018).

9. Pantokratoras, A. Natural convection over a vertical isothermal plate in a non-Newtonian power-law fluid: New results. *Adv. Mech. Eng*. **8**, 1-12 (2016).

10. Mythili, D., R. Sivaraj, R., and Rashidi, M.M. Heat generating/absorbing and chemically reacting Casson fluid flow over a vertical cone and flat plate saturated with non-Darcy porous medium, *Int. J. Numer. Meth. Heat and Fluid Flow*, **27**, 1-20 (2017).

11. Coleman, B. D. and Noll. W. An approximation theorem for functionals, with applications in continuum mechanics, *Archive for Rational Mechanics and Analysis*. **6**, 355-370 (1960).

12. McTigue, D. F., Passman, S.L. and Jones, S. J. Normal stress effects in the creep of ice, *Journal of Glaciology*, **38**, 120–126 (1985).

13. Noor, S. K., Saeed, I., Taza, G., Ilyas K., Waris, K., and Liaqat A. Thin film flow of a second grade fluid in a porous medium past a stretching sheet with heat transfer, *Alexandria Engineering Journal.* (2017).

14. Raftari, B., Parvaneh, F. and Vajravelu, K. Homotopy analysis of the magnetohydrodynamic flow and heat transfer of a second-grade fluid in a porous channel, *Energy.* **59**, 625-632 (2013).

15. Hayat, T., Anwar, M. S., Farooq, M and Alsaedi, A. MHD Stagnation point flow of second grade fluid over a stretching cylinder with heat and mass transfer, *International Journal of Nonlinear Sciences and Numerical Simulation.* **15**, 365–376 (2014).

16. Hameed, M., Khan, A. A., Ellahi, R. and Raza, M. Study of magnetic and heat transfer on the peristaltic transport of a fractional second grade fluid in a vertical tube, *Engineering Science and Technology*, *an International Journal.* **18,** 496-502 (2015).

17. Siddharth, S. B., Amit M., and Gupta, R.S. Mathematical analysis on heat transfer during peristaltic pumping of fractional second-grade fluid through a non-uniform permeable tube, *Journal of Fluids.* **2010**, 1-8 (2010).

18. Hayat, T., Yousaf, A., Mustafa, M., and Obaidat, S. MHD squeezing flow of second-grade fluid between two parallel disks, *Int. J. Numer. Meth. Fluids,* **69**, 399–410 (2012).

19. Misra, J. C., Pal, B. and Gupta, A. S. Hydromagnetic flow of second grade flow in a channel -Applications to physiological system, *Mathematical models and methods in applied in sciences.* **8**, 1323-1342 (1998).

20. Kai-Long Hsiao and Cheng-Hsing Hsu. Conjugate heat transfer of mixed convection for viscoelastic fluid past a horizontal flat-plate fin, *Applied Thermal Engineering.* **29**, 28–36 (2009).

21. Pakdemirli, M., Hayat, T., Yürüsoy, M., Abbasbandy, S. and Asghar, S. Perturbation analysis of a modified second grade fluid over a porous plate, *Nonlinear Analysis: Real World Applications.* **12**, 1774–1785(2011).

22. Umamaheswar, M., Raju, M. C., Varma, S.V.K., Gireeshkumar, J. Numerical investigation of MHD free convection flow of a non-Newtonian fluid past an impulsively started vertical plate in the presence of thermal diffusion and radiation absorption, *Alexandria Engineering Journal.* **55**, 2005–2014 (2016).

23. Masood ur Rahman, Mehwish Manzur and Masood Khan. Mixed convection heat transfer to modified second grade fluid in the presence of thermal radiation, *Journal of Molecular Liquids*. **223**, 217–223(2016).

24. Schlichting, H., *Boundary Layer Theory*, McGraw–Hill, New York, 1979.

25. Harms, T. M., Jog, MA. and Manglik, R. M. Effects of temperature-dependent viscosity variations and boundary conditions on fully developed laminar steady forced convection in a semi-circular duct, *ASME Journal of Heat Transfer*. **120**, 600–605 (1988).

26. Ling, J. X. and Dybbs, A. The effect of variable viscosity on forced convection over a flat plate submerged in a porous medium, *ASME Journal of Heat Transfer*. **114**, 1063-1065 (1992).

27. Molla, M.M., Hossain, M.A., Gorla, R.S. Natural convection flow from an isothermal horizontal circular cylinder with temperature dependent viscosity, Heat Mass Trans., 41, 594 (2005).

28. Gray, J., Kassory, D. R., Tadjeran, H., and Zebib, A., Effect of significant viscosity variation on convective heat transport in water saturated porous media, *Journal of Fluid Mechanics*, **117**, 233–249 (1982).

29. Kafoussius, N. G., and Rees, D. A. S. Numerical study of the combined free and forced convective laminar boundary layer flow past a vertical isothermal flat plate with temperature dependent viscosity, *Acta Mechanica*. **127**, 39–50 (1998).

30. Hossain, M. A., Munir, M. S., and Pop, I., Natural convection flow of viscous fluid with viscosity inversely proportional to linear function of temperature from a vertical cone, *International Journal of Thermal Sciences*. **40**, 366–371 (2001).

31. Wilson, S. K., and Duffy, B. R., Strong temperature-dependent viscosity effects on a rivulet draining down a uniformly heated or cooled slowly varying substrate, *Physics of fluids*. **15**, 827–840 (2003).

32. Elbashbeshy, E. M. A., and Ibrahim, F. N., Steady free convection flow with variable viscosity and thermal diffusivity along a vertical plate, *Journal of Physics D: Applied Physics*. **26**, 2137–2143(1993).

33. Abo-Eldahab, E. M., The effects of temperature-dependent fluid properties on free convective flow along a semi-infinite vertical plate by the presence of radiation, *Heat and Mass Transfer*. **41**, 163–169 (2004).

34. Prasad, K.V., Pal, D., Umesh, V. and Prasanna Rao, N. S. The effect of variable viscosity on MHD viscoelastic fluid flow and heat transfer over a stretching sheet, *Commuication in Nonlinear Science and Numerical Simulation*. **15**, 331–344 (2010).

35. Faraz, N. and Khan, Y. Study of the rate type fluid with temperature dependent viscosity, *Zeitschrift fur Naturforschung*. 67a, 460-468 (2012).

36. Temitope E. Akinbobola and Samuel S. Okoya. The flow of second grade fluid over a stretching sheet with variable thermal conductivity and viscosity in the presence of heat source/sink, *Journal of the Nigerian Mathematical Society*. **34**, 331–342 (2015).

37. Bejan, A. The concept of irreversibility in heat exchanger design: Counter flow heat exchangers for Gas-to-Gas Applications, *Transactions of the ASME*. **99**, 374-380 (1977).

38. Leidenfrost, W., Lee, K. and Korenic, B. Conservation of energy estimated by second law analysis of a power-consuming process, *Energy*, 5,47-61(1980).

39. Ahmet Z. Sahin, Syed M. Zubair, Ahmed Z. Al-Garni, and Ramazan Kahraman. Effect of fouling on operational cost in pipe flow due to entropy generation, *Energy Conversion & Management*, 41, 1485-1496, 2000.

40. Rashidi, M. M., Bég, O. Anwar, Freidoonimehr, N. and Rostami, B. Second law analysis of hydromagnetic flow from a stretching rotating disk: DTM-Padé simulation of novel nuclear MHD propulsion systems, *Frontiers of Aerospace Engineering*, **2**, 29-38 (2013).

41. Giangaspero, G. and Sciubba, E. Application of the entropy generation minimization method to a solar heat exchanger: A pseudo-optimization design process based on the analysis of the local entropy generation maps, *Energy*. **58**, 52-65 (2013).

42. Badescu,V. Optimal paths for minimizing lost available work during usual heat transfer processes, *Journal of Non-Equilibrium Thermodynamics*. **29**, 53-73 (2004).

43. Kockum, H. and Jernqvist, A. Entropy generation in multifield flows: Equations and Examples of Applications, *Institution of Chemical Engineers Trans IChemE*. **76**, 212-222 (1998).

44. Srinivas, J., Ramana Murthy, J.V. and Bég, O. Anwar, Entropy generation analysis of radiative heat transfer effects on channel flow of two immiscible couple stress fluids, *Journal of the Brazilian Society of Mechanical Sciences and Engineering*. **39**, 2191–2202 (2017).

45. Akbar NS, M. Shoaib, D. Tripathi, S. Bhushan and O. Anwar Bég. Analytical approach for entropy generation and heat transfer analysis of CNT-nanofluids through ciliated porous medium, *Journal of Hydrodynamics B* (2018). DOI: 10.1007/s42241-018-0021-x

46. Eger, T., Thomas B., Thanu, A. R., Daróczy, L., Janiga, G., Schroth, R. and Thévenin, D. Application of entropy generation to improve heat transfer of heat sinks in electric machines, *Entropy*. **19**, 1-15 (2017).

47. Oztop HF, Al-Salem K. A review on entropy generation in natural and mixed convection heat transfer for energy systems, *Renew. Sustain Energy Rev.* **16**, 911-920 (2012).

48. Makinde, O. D. and Tshehla, M.S., Irreversibility analysis of MHD mixed convection channel flow of nanofluid with suction and injection, *Global Journal of Pure and Applied Mathematics*. **13**, 4581-4861 (2017).

49. Karim M. C. and John H. L. V, Entropy generation analysis of electrodialysis, *Desalination.* **413**, 184–198 (2017).

50. Nagaraju, G., Srinivas, J., Ramana Murthy, J.V. and Rashad, A.M., Entropy generation analysis of the mhd flow of couple stress fluid between two concentric rotating cylinders with porous lining, *Heat Transfer-Asian Research.* **46**, 316-330 (2016).

51. Srinivas J., Adesanya, S. O., Falade, J.A., Nagaraju, G., Entropy generation analysis for a radiative micropolar fluid flow through a vertical channel saturated with non-Darcian porous medium, *International Journal of Applied and Computational Mathematics*. **3**, 3759-3782 (2017).

52. Shahri, M. F. and Sarhaddi, F., Second law analysis for two-immiscible fluids inside an inclined channel in the presence of a uniform magnetic field and different types of nanoparticles, *Journal of Mechanics*. 1-9 (2017).

53. Chauhan, D. S. and Kumar, V. Entropy analysis for third-grade fluid flow with temperature-dependent viscosity in annulus partially filled with porous medium, *Theoretical and Applied Mechanics*. **40**, 441–447 (2013).

54. Butt, A. S., Munawar, S., Mehmood, A. and Ali, A. Effect of viscoelasticity on entropy generation in a porous medium over a stretching plate, *World Applied Sciences Journal*, 17, 516–523 (2012).

55. Rashidi, M.M., Bagheri, S., Momoniat, E. and Freidoonimehr, N. Entropy analysis of convective MHD flow of third grade non-Newtonian fluid over a stretching sheet, *Ain Shams Engineering Journal*. **8**, 77-85(2017).

56. Porter, R.S. and Johnson, J. F. Temperature dependence of polymer viscosity: The influence of polymer composition, *Journal of Polymer Science Part C: Polymer Symposia*, **15**, 373–380 (1966).

57. Fosdick, R. L. and Rajagopal, K. R. Uniqueness and drag for fluids of second grade in steady motion. *International Journal of Non-Linear Mechanics* **13**, 131–137(1978).

58. Rajagopal, K. R. and Gupta, A. S. An exact solution for the flow of a non-Newtonian fluid past an infinite porous plate, *Meccanica.* **19,** 156-160 (1974).

59. Dunn, J.E., and Rajagopal, K. R. Fluids of differential type: critical review and thermodynamic analysis, *International Journal of Engineering Science.* **33**, 689-729 (1995).

60. Prasad, V. R., Vasu, B., Anwar Bég, O. and Parshad, R. Unsteady free convection heat and mass transfer in a Walters-B viscoelastic flow past a semi-infinite vertical plate: a numerical study, *Thermal Science-International Scientific Journal.* **15**, S291-S305 (2011).

61. Cebeci, T (2002). *Convective Heat Transfer*. Springer, New York, USA.

62. Rani, H. P., Reddy, G. J., and Kim, C. N., 2008, Transient analysis of diffusive chemical reactive species for couple stress fluid flow over vertical cylinder, *Applied Mathematics and Mechanics (English Edition).* **34**, 985–1000 (2013).

63. Takhar, H.S., Ganesan, P., Ekambavanan, K. and Soundalgekar, V.M. Transient free convection past a semi-infinite vertical plate with variable surface temperature, *International Journal of Numerical Methods for Heat and Fluid Flow*. **7**, 280-296 (1997).

64. Bejan, A. *Entropy Generation Minimization. New York: CRC Press* (1996).

TABLES

Grid size	Average $\overline{Nu}$ for $Pr = 0.71, \gamma = 0.3, \beta = 0.2$	Average $\left(-\overline{C_f}\right)$ for $Pr = 0.71, \gamma = 0.3, \beta = 0.2$
25 X 125	0.85652520	0.36779620
50 X 250	0.91484030	0.29038550
100 X 500	0.92885720	0.18117390
200 X 1000	0.92997830	0.18070360

Table 1. Grid independence test for selecting mesh size.

Time step size (Δt)	Average $\overline{Nu}$ for $Pr = 0.71, \gamma = 0.3, \beta = 0.2$	Average $\left(-\overline{C_f}\right)$ for $Pr = 0.71, \gamma = 0.3, \beta = 0.2$
0.5	0.99753640	2.19088000
0.1	0.98363640	1.59130600
0.08	0.97937370	1.44454600
0.05	0.96879970	1.08572900
0.02	0.92986860	0.18888760
0.01	0.92885720	0.18117390

Table 2. Grid independence test for selecting time step size.

FIGURES
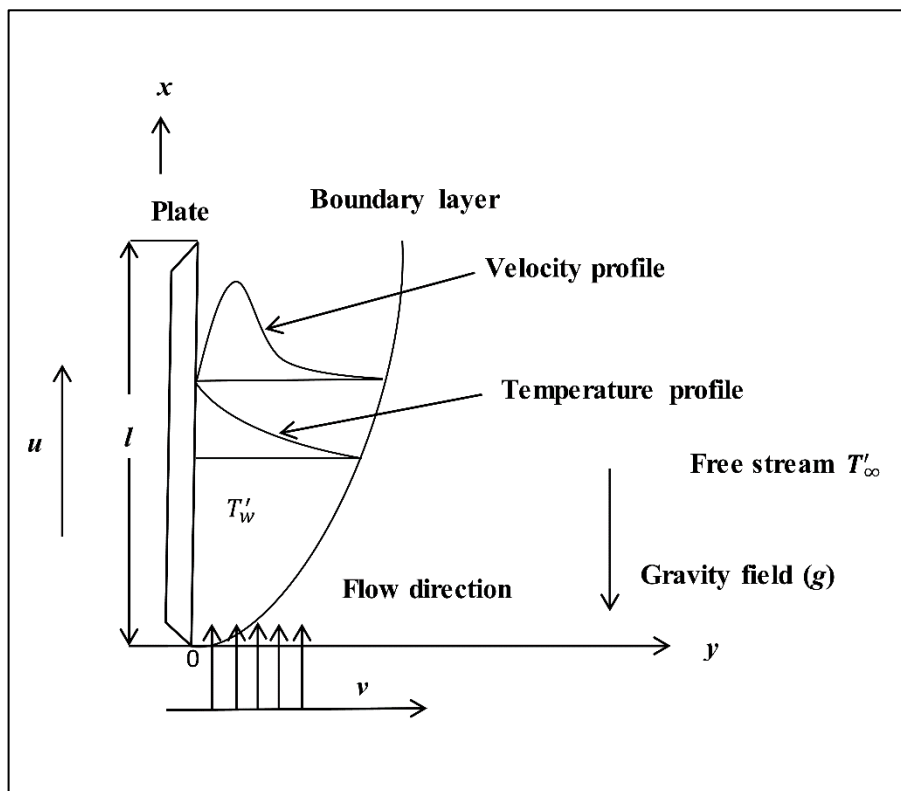
Fig. 1: Flow geometry and coordinate system.
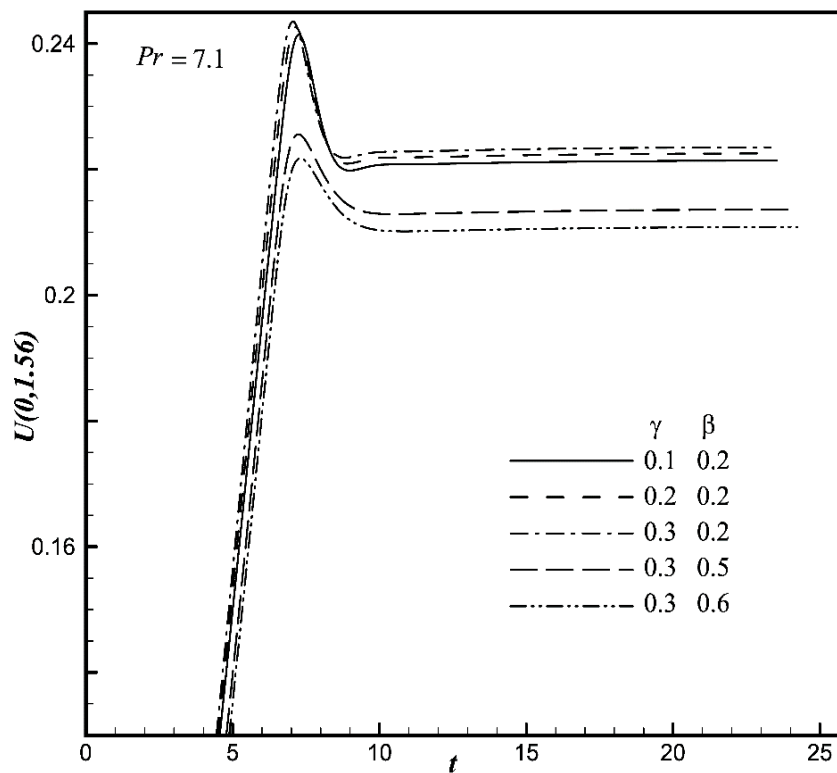
Fig. 2. Comparison of the flow-field variables.
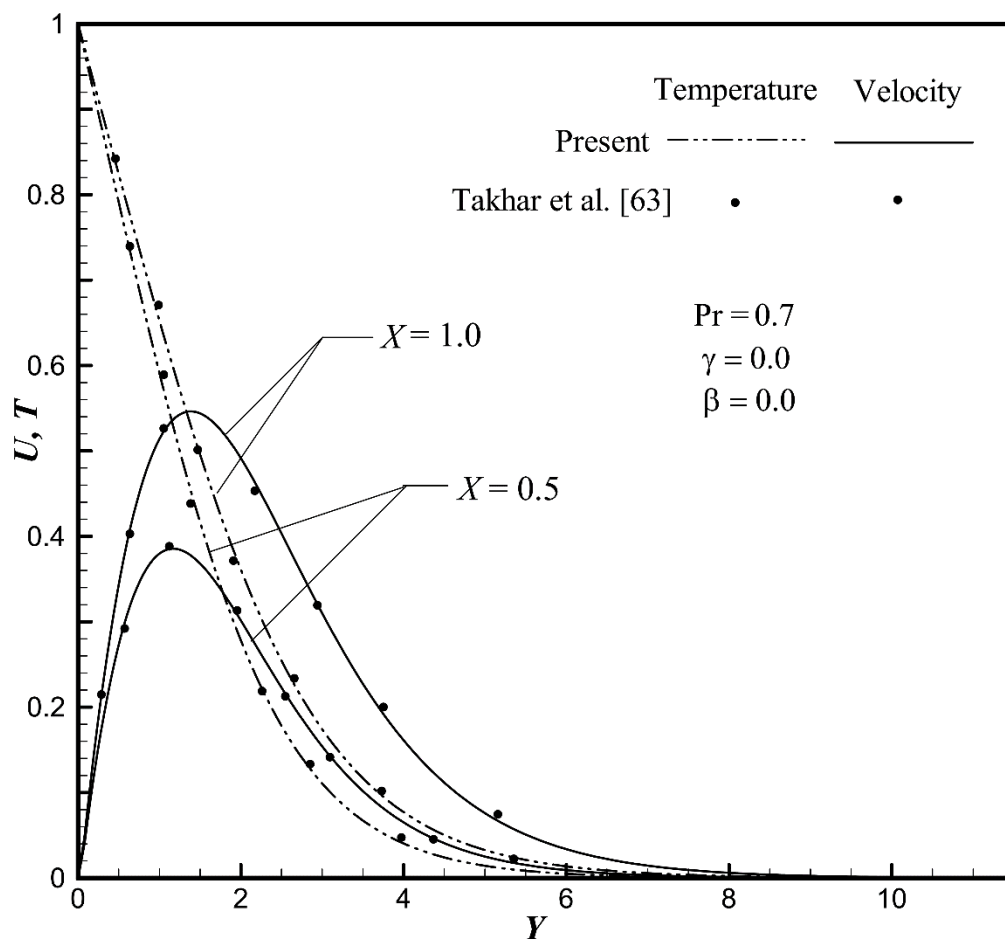
Fig. 3. Time-dependent velocity profile (*U*) versus time (*t*) for various values of γ and β at the location (0, 1.56).
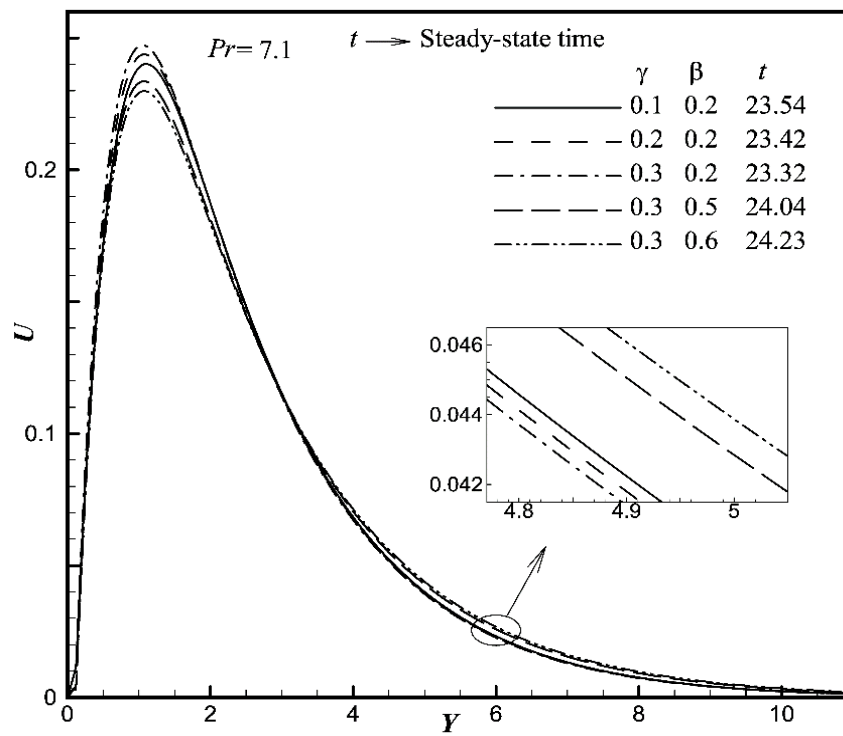
Fig. 4. Simulated time-independent state velocity profile (U) versus Y at $X = 1.0$ for various values of γ and β.
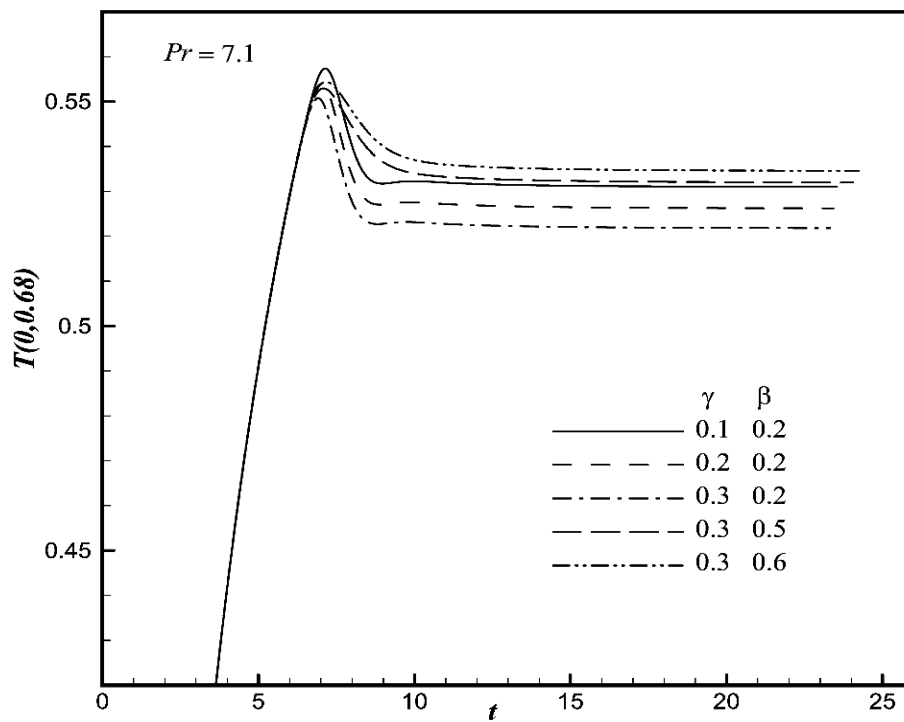
Fig. 5. Simulated time-dependent temperature profile (T) versus time (t) for various values of γ and β at the location (0, 0.68).
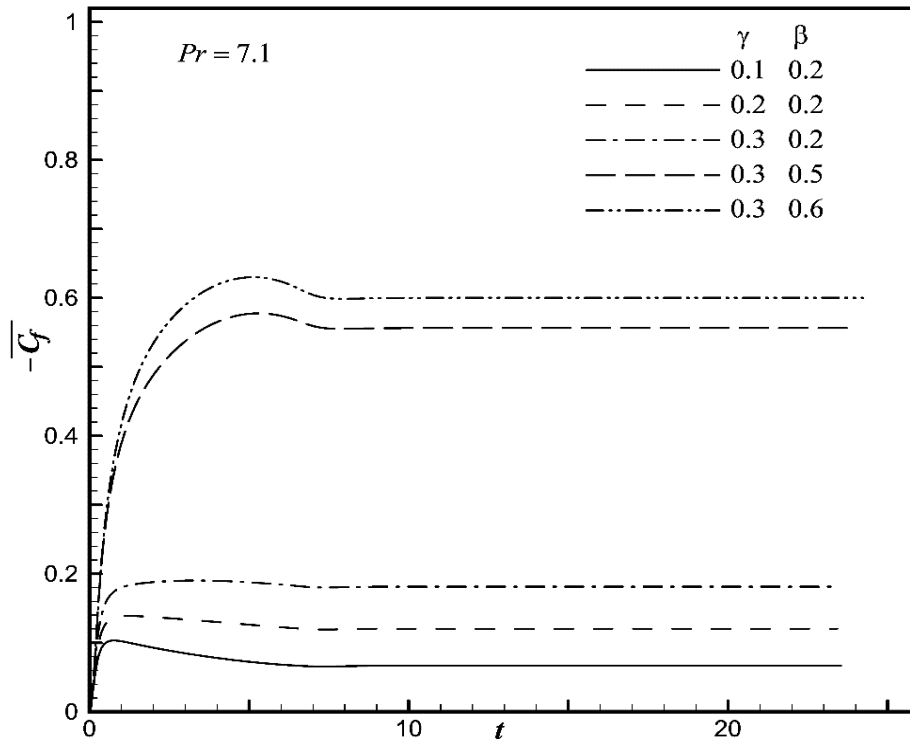
Fig. 6. Simulated time-independent state temperature profile (*T*) versus *Y* at *X* = 1.0 for various values of γ and β.
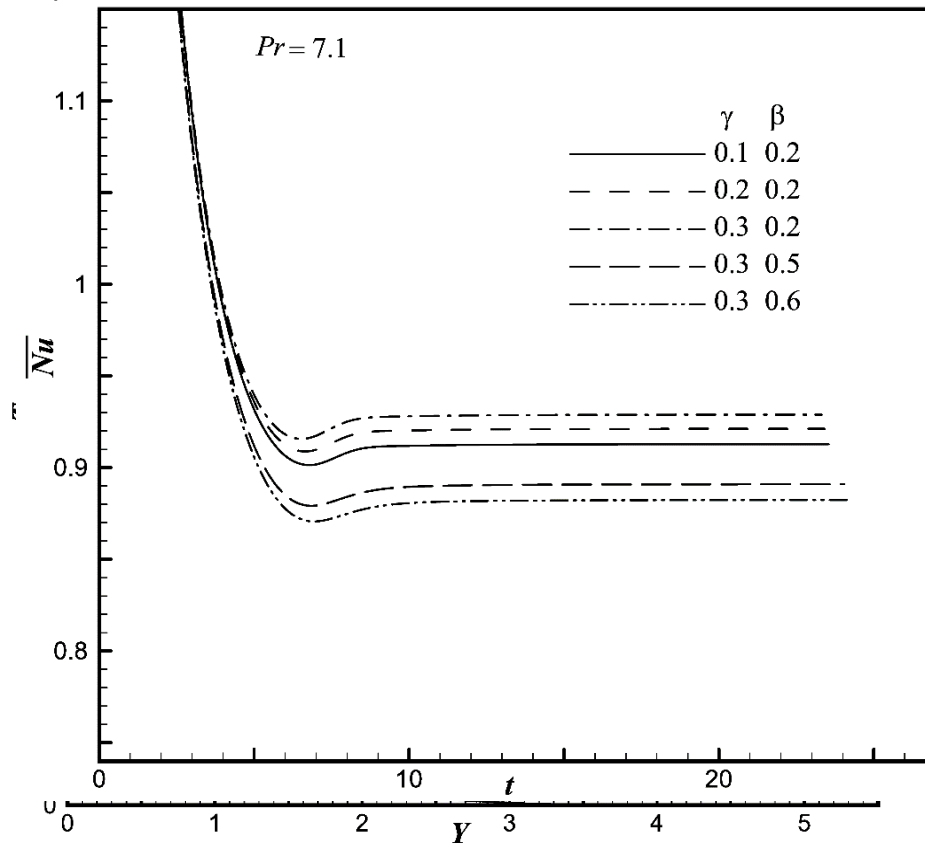
Fig. 7. Average momentum transport coefficient ($\overline{C_f}$) for various values of γ and β.

Fig. 8. Average heat transport coefficient ($\overline{Nu}$) for distinct values of γ and β.
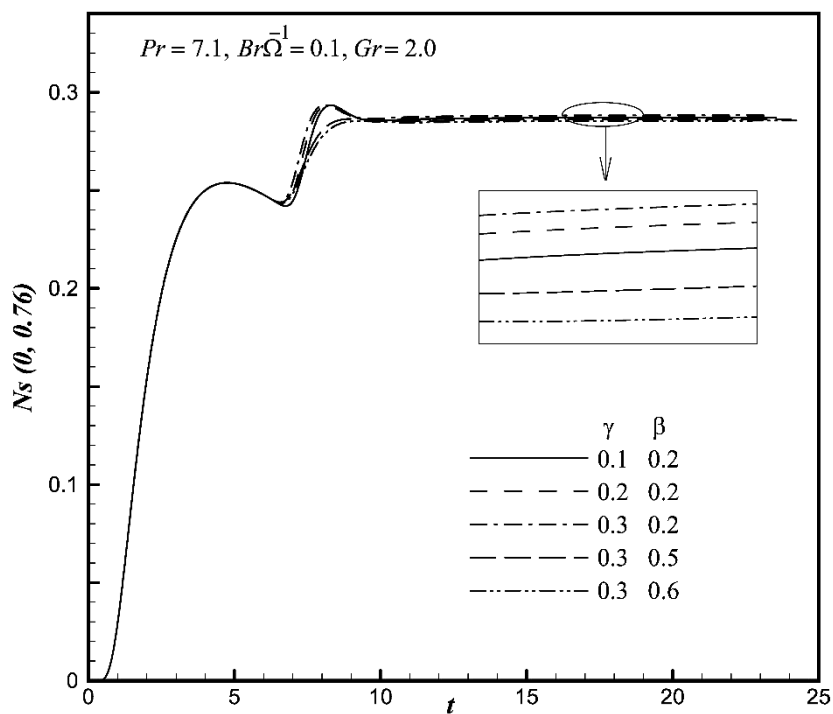
9(a)
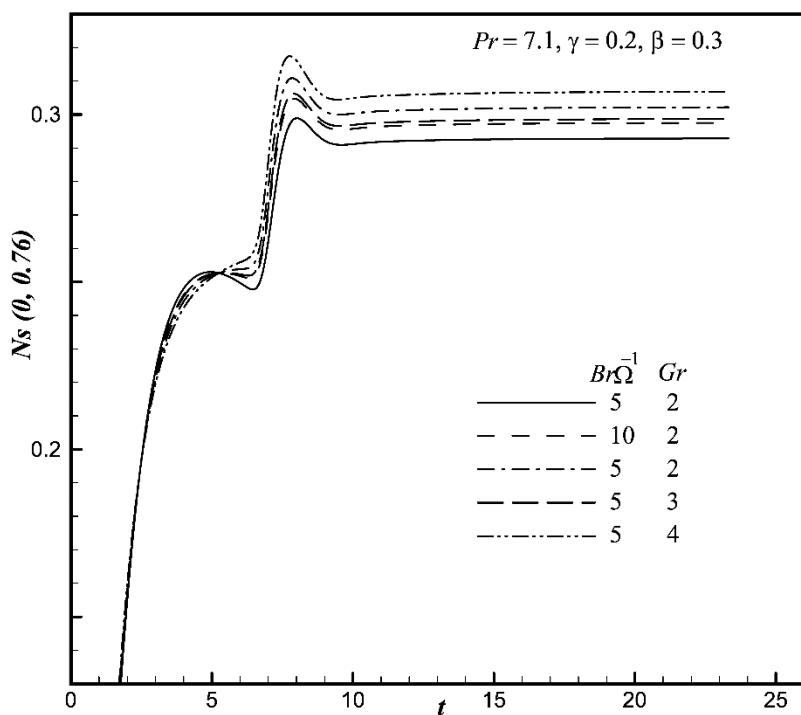
9(b)

Fig. 9. The transient entropy generation number (Ns) against time (t) for different values of (a) γ and β; & (b) $Br\Omega^{-1}$ and Gr.

10(a)

10(b)
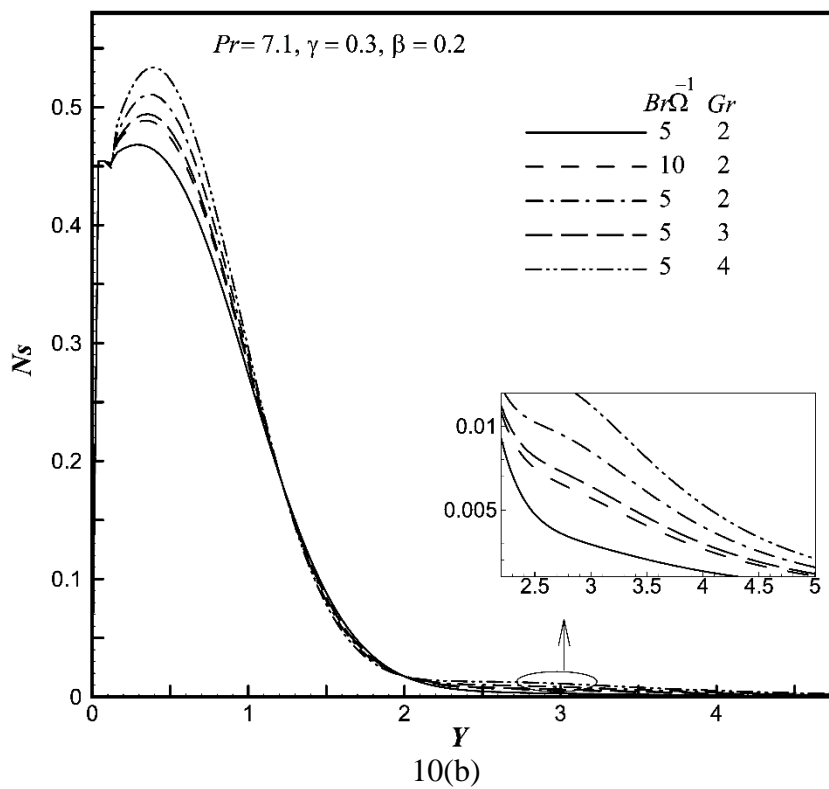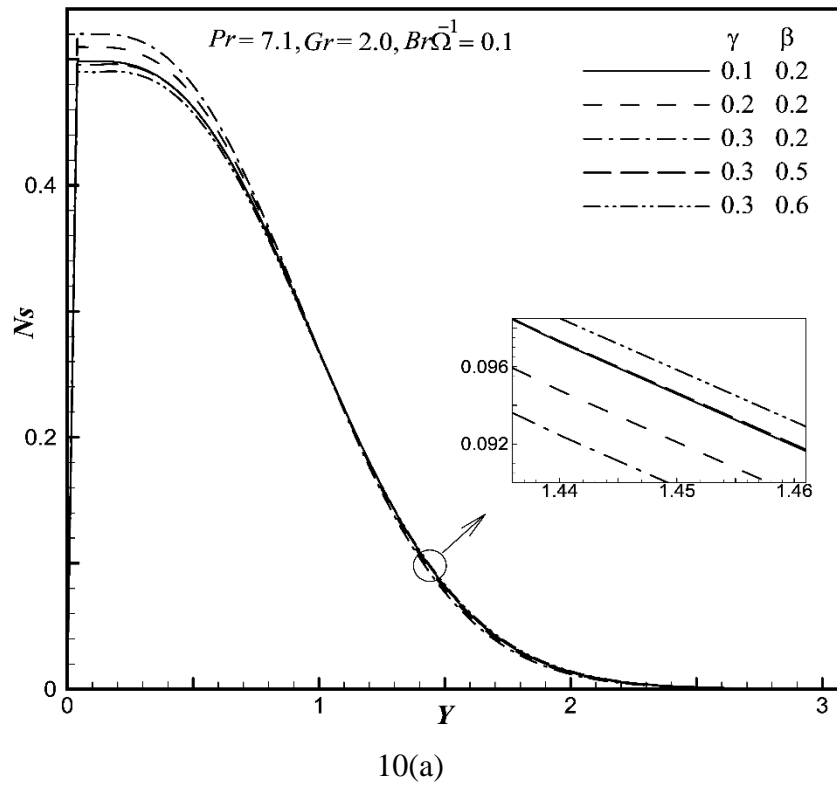
Fig. 10. The steady-state entropy generation number (Ns) against Y at $X = 1.0$ for different values of (a) γ and β; & (b) $Br\Omega^{-1}$ and Gr.
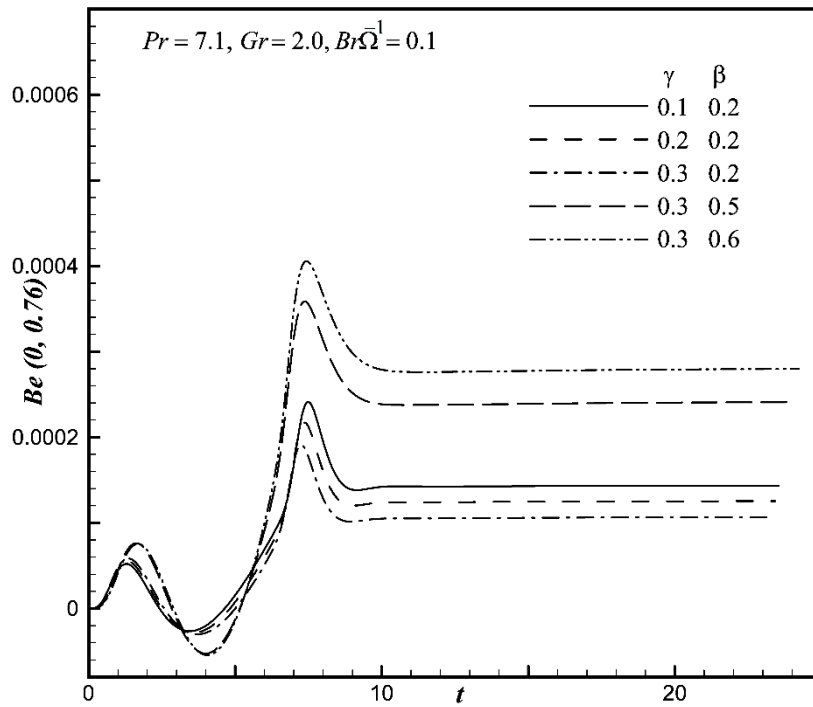
11(a)
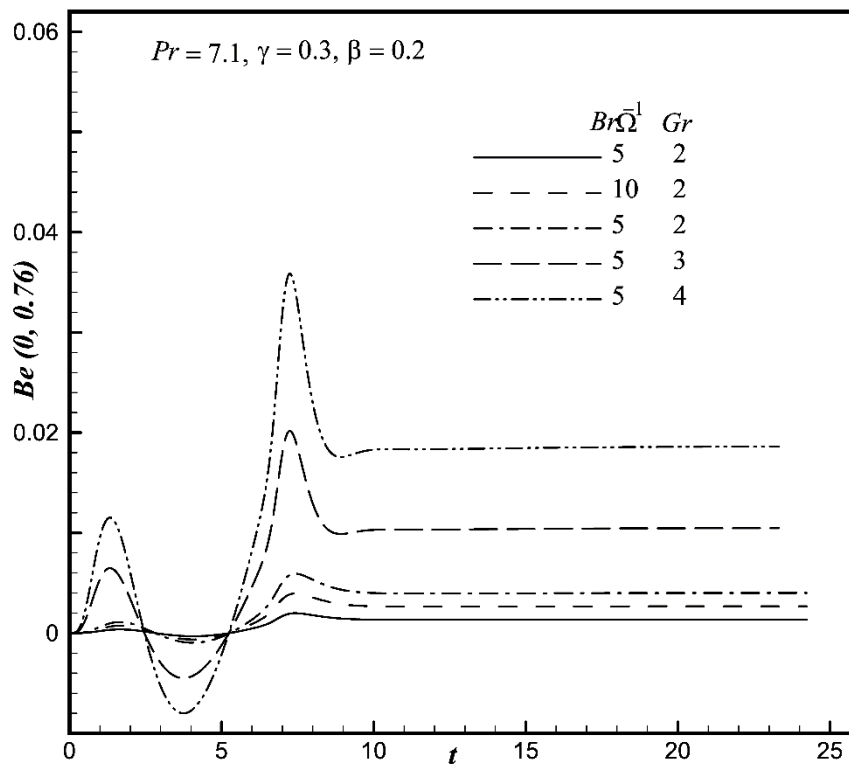
11 (b)

Fig. 11. The transient Bejan number (Be) against time (t) for different values of (a) γ and β; & (b) $Br\Omega^{-1}$ and Gr.

12(a)

12(b)
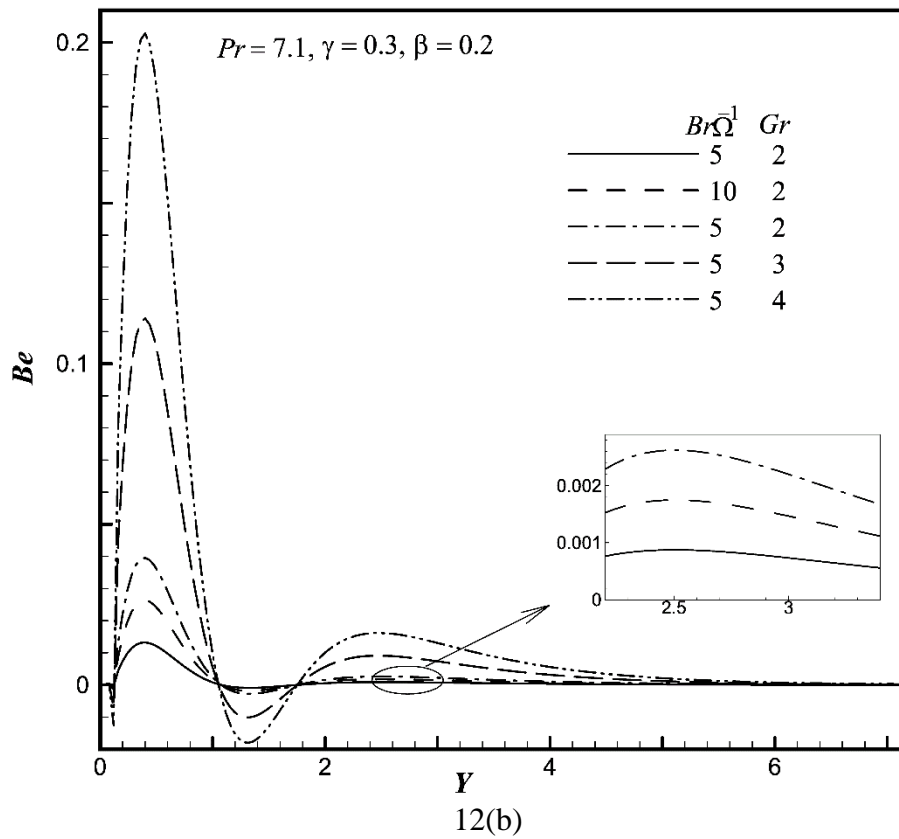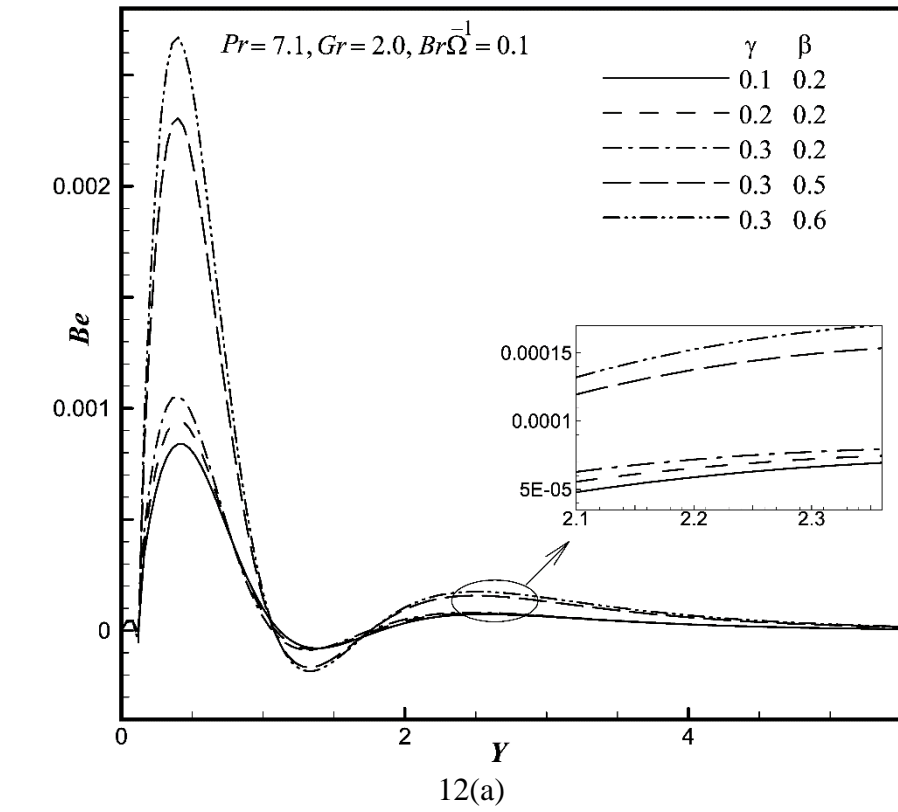
Fig. 12. The steady-state entropy Bejan number (*Be*) versus *Y* at *X* = 1.0 for various values of (a) γ and β; & (b) $Br\Omega^{-1}$ and *Gr*.
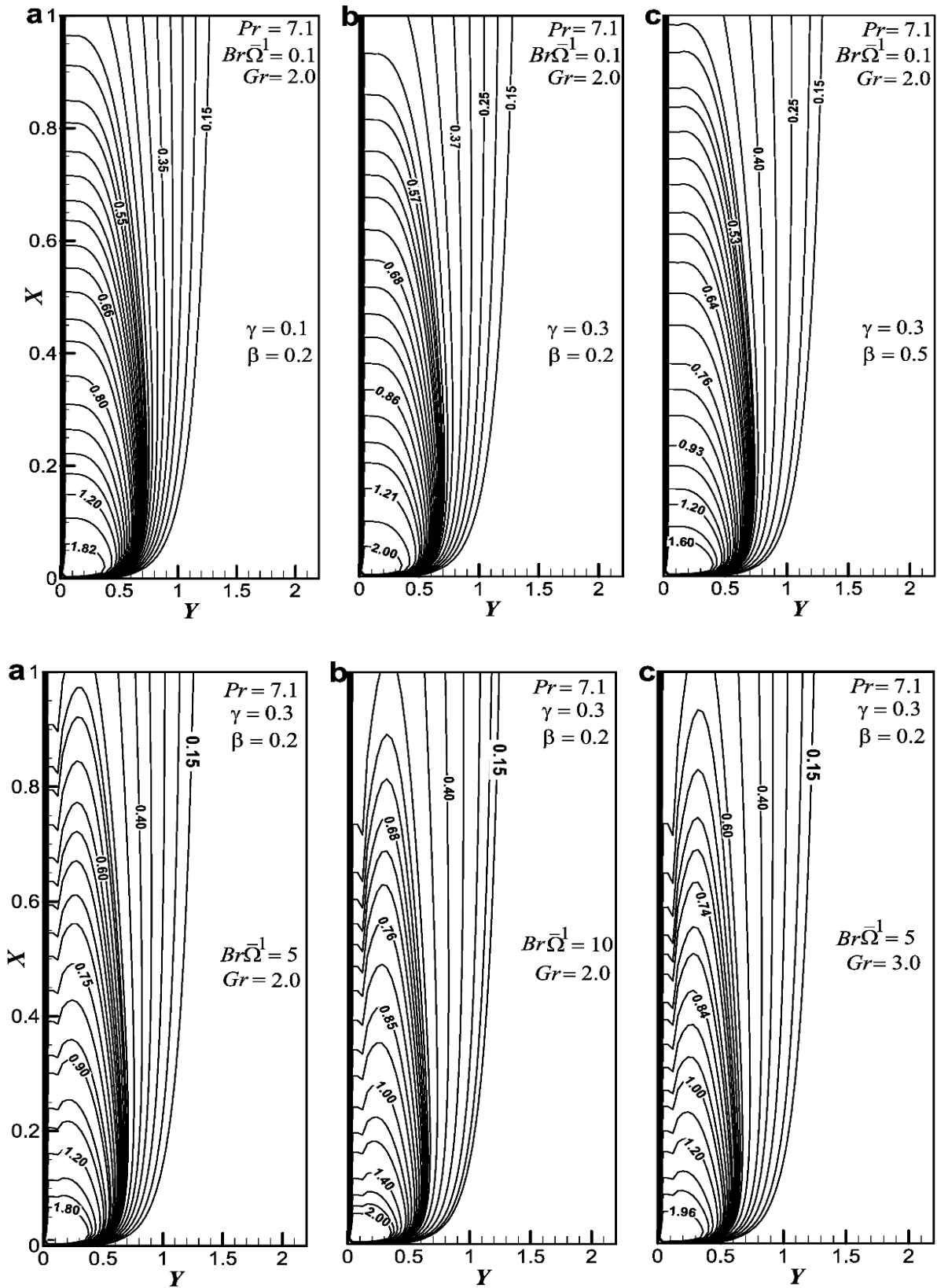
Fig. 13a,b. The steady-state entropy contours (*Ns*) for different values of (a) γ and β; & (b) $Br\Omega^{-1}$ and *Gr*.
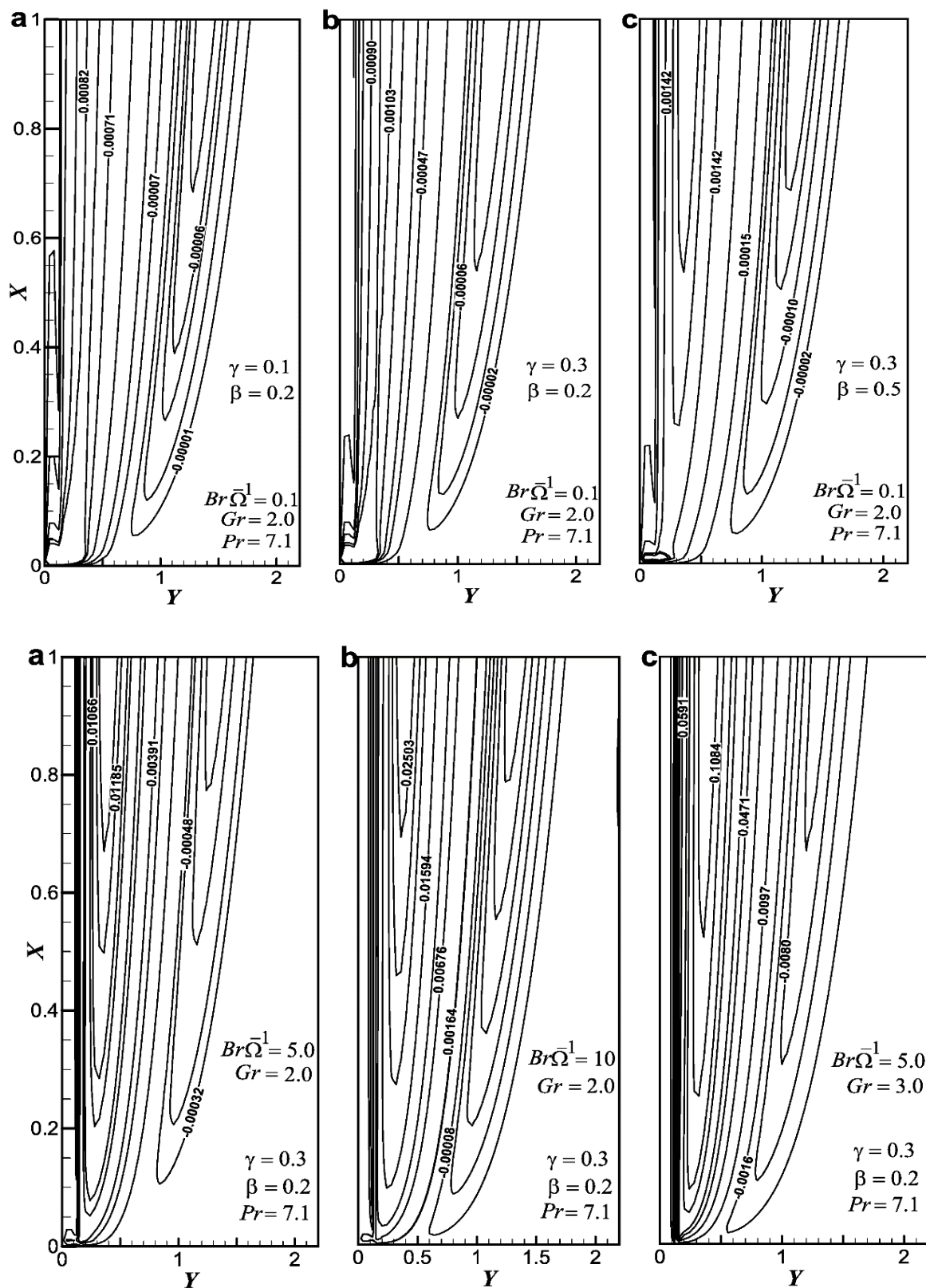
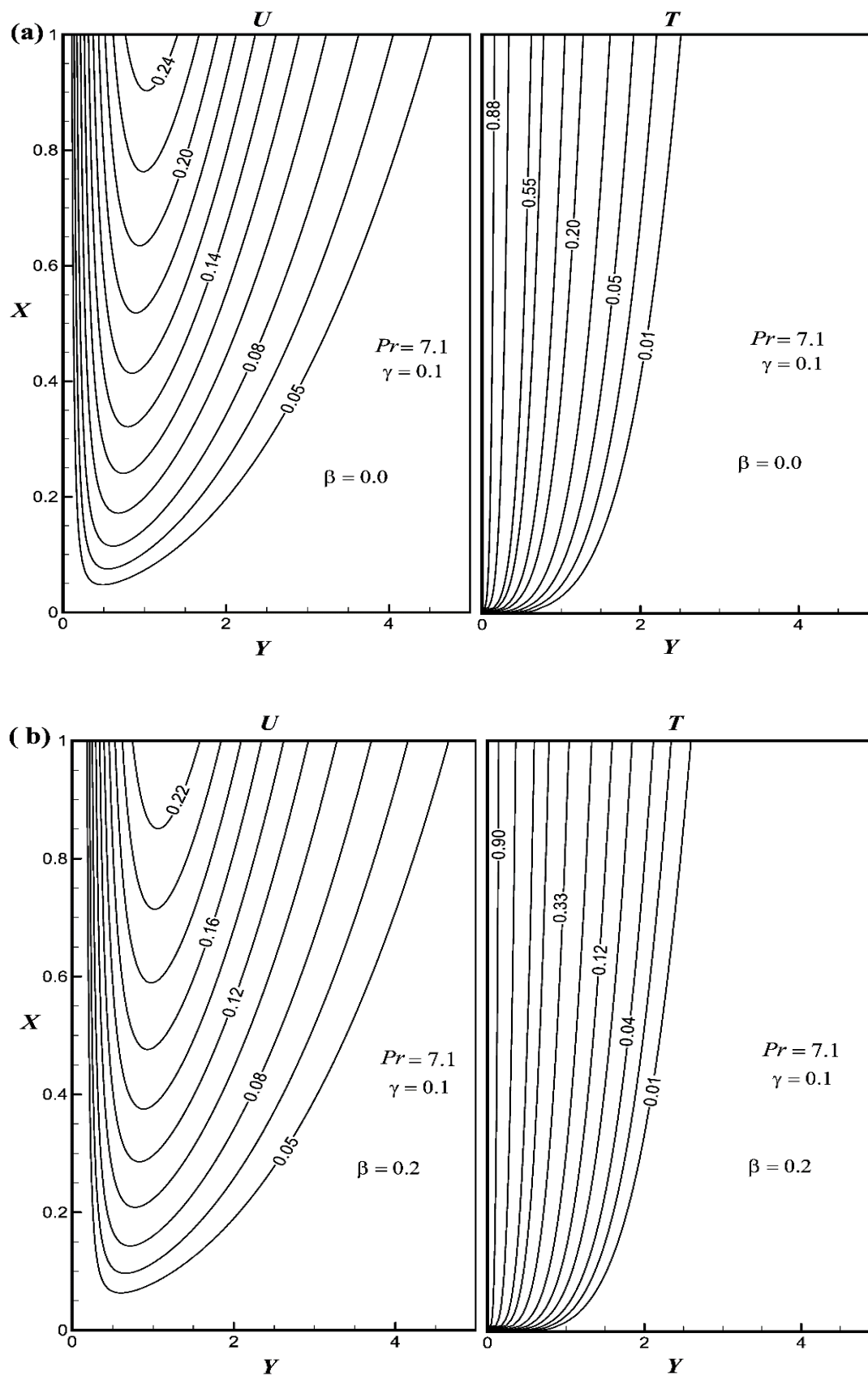Fig. 14a,b. The steady-state Bejan contours (*Be*) for different values of (a) γ and β; & (b) $Br\Omega^{-1}$ and *Gr*.

Fig. 15. The steady-state velocity (*U*) and temperature (*T*) contours for (a) Newtonian fluid (β = 0.0); and (b) second-grade fluid (β = 0.2).